ELEMENTA
Science of the Anthropocene

Mellat, M, et al. 2025. Arctic surface snow interactions with the atmosphere: Spatio-temporal isotopic variability during the MOSAiC expedition. *Elem Sci Anth*, 13: 1. DOI: https://doi.org/10.1525/elementa.2025.00028

RESEARCH ARTICLE

Arctic surface snow interactions with the atmosphere: Spatio-temporal isotopic variability during the MOSAiC expedition

Moein Mellat[1,2,*], Amy R. Macfarlane[3,4,†], Camilla F. Brunello[5,†], Martin Werner[5], Martin Schneebeli[6], Ruzica Dadic[6], Stefanie Arndt[5,7], Kaisa-Riikka Mustonen[8], Jeffrey M. Welker[8,9,10], Dmitry V. Divine[11], and Hanno Meyer[1]

Snow on sea ice is crucial in moderating sea ice and atmosphere interactions, yet fully grasping snow's isotopic composition and the processes shaping it presents substantial challenges, including sublimation and wind redistribution. This study utilizes a year of stable water isotope datasets from the Multidisciplinary drifting Observatory for the Study of Arctic Climate (MOSAiC) expedition in 2019/2020 to explore the complex interactions between snow deposition processes and postdepositional changes affecting snow on Arctic sea ice including seasonal and spatial dynamics. We compare snow data with water vapor isotope measurements by examining 911 individual snow isotope measurements and integrating these discrete snow samples with continuous water vapor isotope data. Autumn shows a pronounced $\delta^{18}O$ offset between snow and vapor. In winter, $\delta^{18}O$ and *d-excess* in surface snow and water vapor diverge sharply, indicating kinetic fractionation under extremely cold temperatures as research vessel Polarstern drifted from the Siberian to the Atlantic Arctic. While water vapor $\delta^{18}O$ responds rapidly to air temperature and humidity changes, surface snow $\delta^{18}O$ values are modulated by postdepositional processes like sublimation and wind redistribution. We found that these 2 processes play a key role in isotopic enrichment that is intensified by the snow's prolonged surface residence. Wind-driven snow redistribution, occurring during 67% of the winter period, leads to an average surface snow $\delta^{18}O$ of −22‰ across the sea ice by redistributing and mixing fresh snow with more metamorphosed snow. This study provides new insights into how wind-driven redistribution and prolonged surface residence not only alter isotopic values in surface snow but also obscure seasonal isotopic patterns, complicating the interpretation of snow isotope records in the Arctic. Our research to understand the differences between the isotopic values of vapor and the isotopic values of snow provides insight into interactions between snow and the atmosphere, as well as the processes that alter isotopic values internally within the Arctic snowpack. Our study highlights the complexity of surface snow isotope geochemistry across the Arctic from the eastern to the central basin during the MOSAiC expedition window and how the underlying processes of water vapor transport, temperature–isotope relations, and the role of secondary processes, including wind redistribution and sea ice formation all contribute to the horizontal and vertical geochemistry patterns.

Keywords: Arctic Ocean, MOSAiC expedition, Snow, Atmosphere, Stable water isotopes

1. Introduction

The Arctic climate system is undergoing rapid transformations, with air temperatures rising 4 times faster than the global average (Rantanen et al., 2022), leading to increased precipitation, atmospheric moistening (Kopec et al., 2016; Vihma et al., 2016), and significant sea ice

[1] Alfred Wegener Institute Helmholtz Centre for Polar and Marine Research, Potsdam, Germany
[2] Institute for Environment Science and Geography, University of Potsdam, Potsdam, Germany
[3] UiT The Arctic University of Norway, Tromsø, Norway
[4] Northumbria University, Newcastle, UK
[5] Alfred Wegener Institute Helmholtz Centre for Polar and Marine Research, Bremerhaven, Germany
[6] WSL Institute for Snow and Avalanche Research SLF, Davos, Switzerland
[7] Institute of Oceanography, University of Hamburg, Hamburg, Germany
[8] Ecology and Genetics Research Unit, University of Oulu, Oulu, Finland
[9] University of the Arctic (UArctic), Rovaniemi, Finland
[10] Department of Biological Sciences, University of Alaska, Anchorage, AK, USA
[11] Norwegian Polar Institute, Tromsø, Norway
[†] These authors contributed equally to this study.
* Corresponding author:
Email: moein.mellat@gmail.com

loss (Jenkins and Dai, 2021; Smith et al., 2023). These changes, driven by extreme events such as warm air intrusions (Klein et al., 2015; Rinke et al., 2021; Brunello et al., 2024), cold air outbreaks (Geerts et al., 2022; Nygård et al., 2023; Hanna et al., 2024), shifting storm tracks (Puntsag et al., 2016; Aemisegger, 2018; Mellat et al., 2021), and enhanced evaporation from ice-free seas (Boisvert et al., 2023), have far-reaching impacts on the Arctic's hydrological cycle and isotope geochemistry, with implications for the global climate system (Zhao et al., 2019; Yamanouchi and Takata, 2020). The interactions between snow and the atmosphere involve feedback loops regulating the Earth's climate at high latitudes (Webster et al., 2018; Feldl et al., 2020). While recent in situ isotope measurements have improved understanding of these processes (Klein et al., 2024; Kopec et al., 2024), gaps remain, particularly regarding snow–atmosphere interactions. This study utilizes an entire year of discrete snow isotope data from Multidisciplinary drifting Observatory for the Study of Arctic Climate (MOSAiC) to investigate seasonal and spatial dynamics, comparing snow data with vapor isotope measurements to better understand deposition and postdepositional processes critical to Arctic atmospheric studies (Reinwarth et al., 1985; Steen-Larsen et al., 2014; Zuhr et al., 2023).

Stable water isotopes ($\delta^{18}O$ and $\delta^{2}H$) can be used as powerful tracers for understanding the complex processes governing snow dynamics in Polar environments (Steen-Larsen et al., 2014; Dadic et al., 2015; Laepple et al., 2018; Ala-aho et al., 2021). We can split the processes determining isotopic values into depositional (e.g., precipitation, atmospheric transport) and postdepositional processes (e.g., sublimation, snow metamorphism, wind redistribution). The vapor exchange between snow and the atmosphere is a depositional process that plays an important role in gradually altering the original meteoric fresh snow signal on Arctic sea ice. Vapor sublimation from snow into the atmosphere and vapor deposition from the atmosphere onto the snow are controlled by local atmospheric conditions and variations in surface heat fluxes. This exchange of vapor between the snow surface and the atmosphere slowly alters the snow's isotope composition, significantly impacting the annual snow surface mass balance and the energy budget (Gong et al., 2023).

Postdepositional processes gradually weaken the correlation between snow isotopes and surface temperature, a phenomenon observed in the snow surface and subsurface layers (Mellat et al., 2024). This weakening highlights the impact of processes such as sublimation, wind pumping, wind redistribution, and snow metamorphism on the snow isotopic value, complicating the interpretation of the original climatic signal (Casado et al., 2018; Laepple et al., 2018). The second-order parameter, deuterium excess ($d\text{-}excess = \delta^{2}H - 8 \times \delta^{18}O$) helps to explore the postdepositional processes in surface snow (Sinclair and Marshall, 2008). Due to the differing sensitivity of $\delta^{18}O$ and $\delta^{2}H$ to kinetic fractionation, *d-excess* is more strongly influenced by surface sublimation, a process in which snow transitions directly into water vapor without passing through the liquid phase, leading to significant isotopic modifications (Beria et al., 2018).

Wind redistributes surface snow, leading to a differential accumulation on sea ice, profoundly affecting the snow's physical and chemical characteristics (Nandan et al., 2023). The Arctic region experiences frequent and powerful wind events capable of transporting snow from several meters to multiple kilometers (Akers et al., 2020). Consequently, deposited Arctic precipitation can mix with snow transported from proximal or distal origins, resulting in its mixing on sea ice. This mixing effect alters the isotopic values of the surface snow, challenging the interpretation of the isotopic composition solely as a direct indicator of local climate conditions (Wahl et al., 2024). The redistributed snow accumulates in ridges. Ridges, elevated structures formed on sea ice through the collision and compression of ice floes, serve as snow deposition zones. This accumulation process enables the ridges to capture up to 22% of all snow cover (Liston et al., 2018), which carries a distinct isotopic value, often more depleted in $\delta^{18}O$ and likely indicative of meteoric origins.

Snow metamorphism is a postdepositional process where snow grains experience structural changes to reach a state of thermodynamic stability (Colbeck, 1980; Vérin et al., 2022). This metamorphism occurs at the surface and within the snow profile and, under certain conditions, is largely driven by temperature gradients inducing vapor transport (Pinzer and Schneebeli, 2009). Snow metamorphism begins when there is an internal temperature gradient between the upper and lower parts of the snowpack, contributing to enhanced thermodynamic instability and triggering substantial shifts in the snow isotopic composition through vapor condensation and sublimation processes (Legagneux and Domine, 2005; Harris Stuart et al., 2023; Macfarlane et al., 2023b). Additionally, isothermal metamorphism, although playing a minor role in Arctic sea ice, can also contribute to snow-grain changes under uniform temperature conditions (Colbeck, 1980). During the Arctic melt season, 2 distinct but concurrent phenomena occur: wet-snow metamorphism and the formation of a surface scattering layer on the sea ice surface. The first process impacts the albedo, where the snow grains coarsen and reduce their scattering coefficient. Second, the highly reflective snow cover melts and exposes the less-reflective underlying sea ice to solar radiation. The intense absorption of solar radiation leads to the formation of a porous, granular, and extremely fragile pillared structure atop the melting sea ice, known as the surface scattering layer (Light et al., 2022; Macfarlane et al., 2023a). The presence of this layer and its high porosity facilitates the infiltration of freshwater into the upper layers of the sea ice, associated with a change in snow's isotopic composition.

This manuscript uses combined measurements of stable water isotopes of discrete snow samples and continuous water vapor measurements collected during the MOSAiC expedition between September 2019 and October 2020. This dataset, covering a full year, was built to observe the interactions between physical and chemical processes at the snow–atmosphere interface. In this study,

we examine the seasonality of the interaction between snow and atmosphere during MOSAiC, focusing on the isotopic compositions of the uppermost layer of snow. Besides vapor isotope measurements, we use complementary data on precipitation events from continental stations to compare with the isotopic composition of snow accumulating atop sea ice, aiming to link the Central Arctic processes to the coastal sites.

2. Methods

2.1. The MOSAiC expedition

The MOSAiC expedition consisted of a year-long drifting expedition across the Central Arctic. The German research vessel Polarstern (PS) set sail from Tromsø, Norway, on September 20, 2019, ending its mission in Bremerhaven, Germany, on October 12, 2020. This expedition was subdivided into 5 stages or "legs" (Nicolaus et al., 2022). PS, anchored to a selected ice floe, which served as a dynamic platform for, among many other studies, continuous snow observations, particularly during the initial 3 legs of the expedition (from October 2019 to mid-May 2020). After a logistical detour to Svalbard on May 16, 2020, the expedition's focus on snow research persisted when PS returned to the ice on June 17, 2020, and continued summer measurements until the floe broke up on July 31, 2020. For concluding summer investigations, PS went back to the Central Arctic Ocean, near the north pole (87°N, 104°E), to conduct further measurements in August and September 2020.

2.2. Snow sample collection and laboratory analysis

2.2.1. MOSAiC snow isotope and physical properties

During the MOSAiC expedition, a comprehensive snow survey was conducted, collecting 304 snow samples from various profiles. Snow samples were gathered from 3 specific layers within the snow profiles: surface, middle, and bottom (Mellat et al., 2022). The surface layer was in direct contact with the air, the middle layer was situated approximately halfway through the snow profile, and the bottom layer was directly above the sea ice surface. These samples, varying in depth due to the variable snow cover thickness, were collected using a density cutter, stored in sampling bags, and maintained frozen until laboratory analysis. The collected samples were thawed at room temperature prior to isotope analyses later in the laboratory.

These samples were processed and analyzed at the ISOLAB facility of the Alfred Wegener Institute Helmholtz Centre for Polar and Marine Research (AWI) in Potsdam, Germany. Here, the stable water isotopic composition, specifically $\delta^{18}O$ and $\delta^{2}H$, was determined. Samples were thawed, transferred into 20 ml glass vials, sealed with parafilm tape, and stored at 4°C for subsequent isotopic analysis using mass spectrometers, employing equilibration techniques for high precision with an accuracy of better than ±0.1‰ for $\delta^{18}O$ and ±0.8‰ for $\delta^{2}H$ (Meyer et al., 2000).

Determining $\delta^{18}O$ and $\delta^{2}H$ involves calculating the isotopic ratio of heavy to light isotopes, compared to a standard, Vienna-Standard Mean Ocean Water (V-SMOW), and presenting the difference in parts per thousand (per mil; ‰). In this study, we use delta (δ) notation which gives the sample's isotope ratio compared to that of the V-SMOW. Additionally, the *d-excess*, a second-order parameter, is calculated using the equation $\delta^{2}H - 8 \times \delta^{18}O$ (Craig, 1961). The *d-excess* is considered to be indicative of moisture source conditions such as sea surface temperature and wind speed (Merlivat and Jouzel, 1979) but also reflects kinetic fractionation related to secondary, postdepositional processes such as evaporation or sublimation (Beria et al., 2018).

2.2.2. Precipitation events from continental stations

The Pan-Arctic Precipitation Isotope Network (PAPIN) was established in 2018 to improve our understanding of the Arctic hydrological cycle using stable water isotope observations (Mellat et al., 2021). The sample network includes more than 30 strategically distributed stations spanning different Arctic climate zones, such as tundra, subarctic, maritime, and continental zones (Mellat et al., 2021). In this study, we use stable water isotope data from event-based precipitation samples from 2 PAPIN stations during the time of the MOSAiC expedition. Samoylov Island (72°N, 126°E) and Ny-Ålesund (78°N, 11°W) stations were selected due to their proximity to the track of the MOSAiC expedition and their extensive data coverage. Samoylov Island is the closest continental station from the start of the MOSAiC drift track in October 2019, and it is situated approximately 1,450 km to the south. Similarly, Ny-Ålesund is located within a range of 200–550 km from PS in June and July 2020. Both stations provide spatial context for interpreting the MOSAiC observations.

Between October 2019 and October 2020, 90 precipitation events were collected at Samoylov Island and 25 at Ny-Ålesund, between May and September 2020. Each station was equipped with a precipitation gauge placed 0.5–1.5 m above the ground, and samples were collected immediately after each event. These were then stored in plastic screw-cap vials and refrigerated at 4°C after sampling. The date, time, air temperature, and precipitation amounts were documented for each event. For isotopic measurement, the samples were transferred to 2 ml septa-capped glass vials (for Ny-Ålesund), and 30 ml narrow-neck PE bottles (for Samoylov Island), and analyzed for their $\delta^{18}O$ and $\delta^{2}H$ isotopes at the isotope labs at the University of Oulu, Finland (for Ny-Ålesund), and ISOLAB at AWI Potsdam (for Samoylov Island) with similar measurement precisions of better than ±0.1‰ for $\delta^{18}O$ and ±0.8‰ for $\delta^{2}H$.

2.3. Complementary data

2.3.1. Vapor isotope measurements during MOSAiC

In addition to the snow isotope dataset, continuous, high-resolution measurements of stable water isotopes of vapor were included in the analysis (Brunello et al., 2022a). These measurements were acquired through a Picarro L2140-i Cavity Ring-Down Spectrometer (CRDS) installed at around 29 m above the sea ice level, which was operational throughout the entire campaign. This setup yielded a comprehensive dataset, including humidity, $\delta^{18}O$, and $\delta^{2}H$ (Brunello et al., 2023).

2.3.2. Meteorological data

To assess the influence of meteorological conditions on the surface snow isotopes, we used the final, processed (Level 3) measurements and derived parameters collected from an array of instruments located at the Meteorological (Met) City site within the Central Observatory of MOSAiC (Cox et al., 2023). These data included air temperature (T) at 2 m above the sea ice surface, relative humidity (RH) at 2 m, latent heat flux (LHF) measured at 10 m, and wind speed (WS) at 2 m. Additionally, precipitation amounts along the trajectory of PS were extracted from the gridded European Centre for Medium-range Weather Forecasts (ECMWF) fifth-generation reanalysis (ERA5) dataset (Hersbach et al., 2020).

2.3.3. Long-term vapor and precipitation isotope data from continental stations

To complement our dataset, we also analyzed long-term simultaneous isotope data of vapor and precipitation from previous studies conducted at 2 continental stations, Samoylov Island and Ny-Ålesund. It is noteworthy that observation periods of the long-term data at these 2 stations do not overlap. In the Lena River Delta in north-east Siberia, specifically at the research station on Samoylov Island, vapor and precipitation data were collected (Bonne et al., 2020). A CRDS continuously recorded the near-surface water vapor isotopic composition from 2015 until 2017. Precipitation sampling was conducted after each rainfall and snowfall event. In Ny-Ålesund, 2 Picarro CRDS were deployed (analyzing water vapor at 8 m above sea level), at the AWIPEV observatory building (Leroy-Dos Santos et al., 2020). A L1102-i Picarro instrument was operational from May 2014 to May 2015, a L2130-i Picarro instrument replaced the first device and continued the measurements until the end of the campaign in September 2018. During precipitation events, water or snow was sampled daily at midday. Over the 4.5 years, a total of 519 precipitation samples were collected and analyzed for their stable water isotopes, offering a detailed long-term perspective on isotopic variations in the region.

3. Results

Our results disentangle spatial and temporal variations in the isotopic values of Arctic snow, including how it is deposited and altered afterward. We do this by initially looking at the temporal signal and seasonality of the dataset (Section 3.1) by comparing the vapor and snow surface isotopic values in the high Arctic. To confirm this signal is not a result of the MOSAiC drifting across the Arctic basin with large changes in location, we investigate the isotopic compositions of $\delta^{18}O$ and *d-excess* of event-based precipitation, sampled at 2 continental stations: Samoylov Island and Ny-Ålesund (Section 3.2). The former is located on the northern coast of Siberia, whereas the latter is located on Svalbard at the eastern entrance to the Fram Strait.

3.1. Seasonality of isotope variations in snow profiles throughout the MOSAiC expedition

This study investigates the seasonal variation of $\delta^{18}O$ values in snow samples collected during the MOSAiC expedition from October 2019 to September 2020. **Figure 1** illustrates the relationship between snow height and isotope variations in the snow on the sea ice. **Figure 1** reveals distinct seasonal shifts in snow height and snow isotopic composition.

In winter, from October to December 2019, $\delta^{18}O$ values (**Figure 1a**) are slightly above −5‰. In January and February 2020, higher $\delta^{18}O$ values are pronounced, particularly in the lower layers of the snow by up to 0‰, near the snow–sea ice interface. Conversely, predominantly lower $\delta^{18}O$ values are observed in the upper layers of snow from January to May 2020, which may reach down to around −30‰.

In summer, June to August 2020 snow samples display predominantly higher $\delta^{18}O$ values, which persist mostly in the lower layers of snow, but the contrast top-to-bottom is less pronounced. At the same time, the snow height decreased significantly to values below 30 cm from August onward.

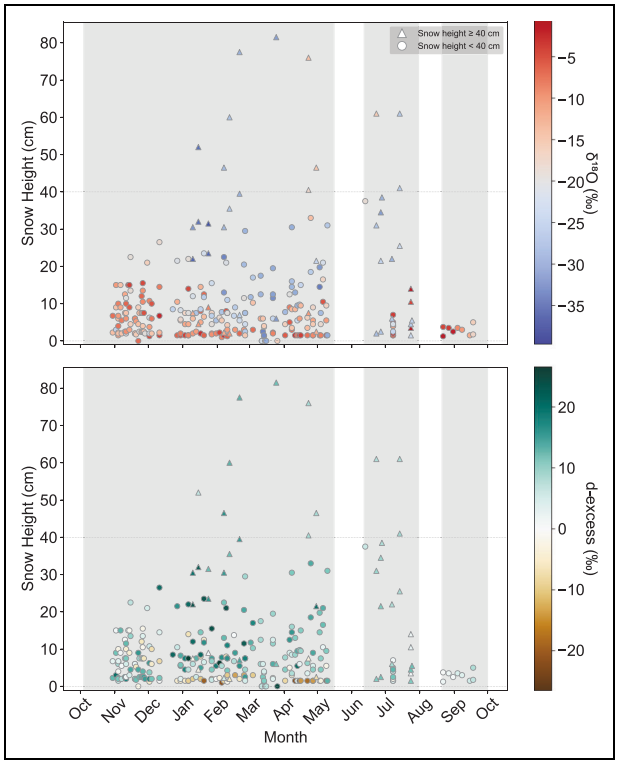

Figure 1. Snow profile samples collected during the MOSAiC expedition from October 2019 to September 2020. (a) $\delta^{18}O$ values are plotted against the snow height for each sample. Samples above 40 cm, in general, represent snow accumulated on ridges, indicated by triangle symbols. Samples from snow heights below 40 cm are represented by circles. (b) Shows the corresponding *d-excess* across the snow height, with triangles to represent snow at the ridges and circles for flat ice areas. Gray-shaded areas in the background of both panels represent periods when the PS was frozen in the Arctic Ocean's sea ice, during which sampling was systematically conducted. White areas signify the intervals of transit between different segments of the expedition.

The negative *d-excess* values confirm the snowpack's thermal variability: the early months (October to December 2019) are characterized by a mix of positive and negative values (−10‰ to 10‰) across most samples. However, there are positive values (up to +20‰), especially at the surface of the snowpack. The *d-excess* variability increases in January and February 2020, with increasing snow height showing a large isotopic gradient between bottom and surface snow (Macfarlane et al., 2023b). During this period, the lower layers of the snow cover near the sea ice interface predominantly exhibit negative *d-excess*, while the upper layers show positive values. The period between January and April displays some of the highest positive *d-excess* values recorded during the entire expedition, exceeding +20‰ in some instances. In contrast, during the summer months, in June and July 2020, the *d-excess* variability decreases toward 0‰ to 10‰. Overall, the $\delta^{18}O$ and *d-excess* trends throughout the MOSAiC year exhibit a periodic pattern with similarities between early and late stages and higher variability in between, which are accompanied by changes in snow height (Supplementary Figures S1 and S2).

3.2. Snow and vapor $\delta^{18}O$ during MOSAiC

To identify key factors driving the interaction between atmosphere and snow, we compare $\delta^{18}O$ in surface snow ($\delta^{18}O_{Snow}$) with a continuous $\delta^{18}O$ times series in water vapor ($\delta^{18}O_{Vapor}$). Both datasets were averaged to monthly means and compared to aggregated weekly precipitation amounts (**Figure 2**). The number of snow samples collected at the surface during each month varies from 2 samples (June, July, August, September 2020) to 24 samples in November 2019.

Although PS drifts southward from 87°N between October 2019 and July 2020 and then returns to 89°N in August 2020 (**Figure 3a**), $\delta^{18}O_{Snow}$ and $\delta^{18}O_{Vapor}$ show a distinct seasonal cycle (**Figure 2**, Supplementary Figures S1 and S2). The seasonal cycle in the surface snow samples is as follows: upper $\delta^{18}O_{Snow}$ values reach a maximum of −3‰ in August 2020 to December 2019, decreasing to the absolute minimum of −33‰ in March 2020 (Table S1). Then, median $\delta^{18}O_{Snow}$ values rose to the absolute maximum of −3‰ in August 2020, with a decrease to ca. −13‰ in September 2020, where samples mostly consisted of the surface scattering layer. The summer months show the largest variability in $\delta^{18}O_{Snow}$ −31‰ and −3‰ in June and August, respectively. The colder months' $\delta^{18}O_{Snow}$ vary less with median values of −17‰ (January 2020), −18‰ (February 2020), and −25‰ (March 2020).

Transitioning to describe the seasonal cycle of the vapor samples, we see the $\delta^{18}O_{Vapor}$ display generally lower values, decreasing slightly from a maximum in October 2019 ($\delta^{18}O_{Vapor} = -37$‰, s.d. = 5.6‰) to the absolute minimum $\delta^{18}O_{Vapor}$ in March 2020 ($\delta^{18}O_{Vapor}$ of ca. −43‰, s.d. = 4.3‰). Afterward, the median $\delta^{18}O_{Vapor}$ values increased continuously to the absolute maximum in August 2020 ($\delta^{18}O_{Vapor} = -18$‰, s.d. = 4.6‰). In September 2020, when PS moved to a more northward

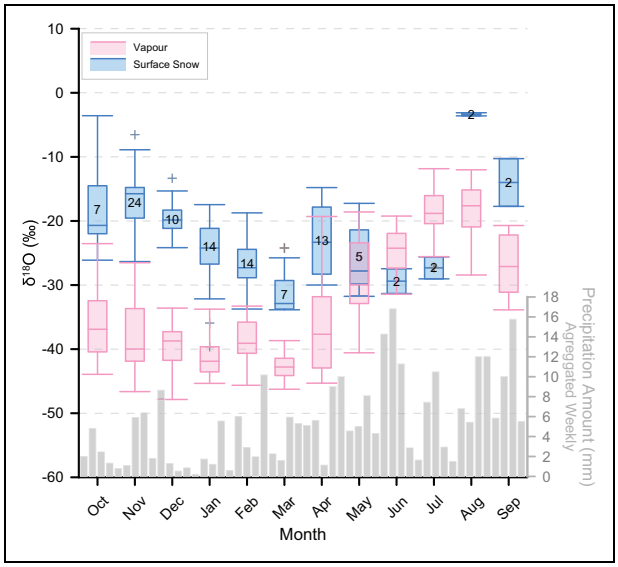

Figure 2. Monthly $\delta^{18}O$ variations for vapor (pink) and surface snow (blue) during the MOSAiC expedition (October 2019 to September 2020). Monthly median values of $\delta^{18}O$ are indicated by the central line within each boxplot, while the box edges correspond to the 25th and 75th percentiles. Whiskers extend to the non-outlier maximum and minimum values, with outliers depicted as plus symbols. The number of samples analyzed for each month is given in the boxes. The weekly aggregated precipitation amounts, derived from the ERA5 reanalysis within the respective moving grid box of PS, are depicted as gray bars in a time series.

position, the median of $\delta^{18}O_{Snow}$ and $\delta^{18}O_{Vapor}$ both decreased by 10‰.

Despite the general similar seasonal evolution of $\delta^{18}O_{Snow}$ and $\delta^{18}O_{Vapor}$, there is a noticeable offset in their trends, and throughout the expedition, the median $\delta^{18}O_{Vapor}$ remains lower than $\delta^{18}O_{Snow}$. This is apparent especially in winter where, the $\delta^{18}O_{Vapor}$ values are stable and range from −32‰ to −45‰, while $\delta^{18}O_{Snow}$ shows a continuous decrease from about −6‰ to −25‰ from November 2019 to March 2020. This isotope difference between vapor and snow median $\delta^{18}O$ values reaches 16‰ in October 2019, increasing to a largest offset of 24‰ in November (Table S1), then decreasing from 19‰ in December 2019 to 9‰ in March 2020. The minimal isotope difference between vapor and snow ranges between 5‰ and 8‰ between June and July 2020 and increases again to 13‰ in September 2020. This divergence between $\delta^{18}O_{Snow}$ and $\delta^{18}O_{Vapor}$ in winter and convergence in summer suggests a seasonal behavior, where the isotopic composition of surface snow responds differently to water vapor during specific periods, possibly influenced by distinct environmental factors.

The aggregated weekly precipitation amounts, derived from the ERA5 reanalysis within the respective moving grid box of PS, exhibit higher values in the summer months compared to winter. In months with consistently higher precipitation amounts, particularly from May

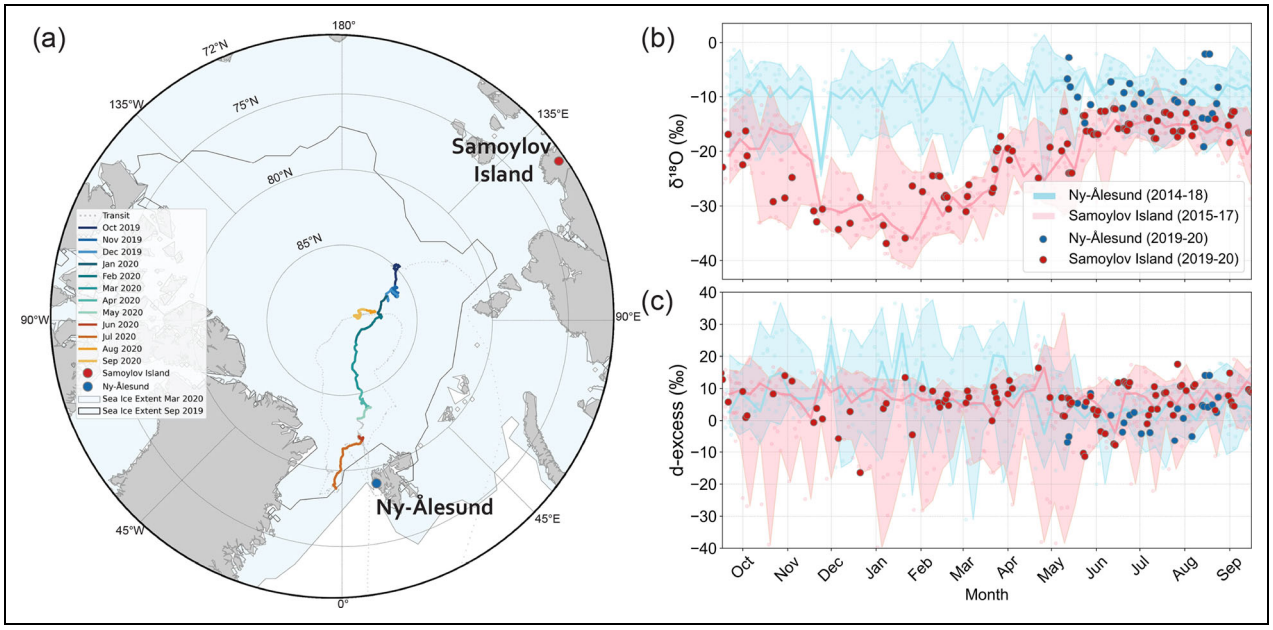

Figure 3. Polar projection of the Arctic Ocean with PS's track during the MOSAiC expedition color-coded by months; transit periods are represented by gray dots. (a) Locations of event-based precipitation sampling on Samoylov Island and at Ny-Ålesund stations are indicated. The sea ice extent at annual maximum and minimum (MOSAiC year) is depicted in light blue shading. (b) and (c) Present $\delta^{18}O$ and *d-excess* measurements of sampled precipitation events for an annual cycle from October to September for both stations. Light blue and light red shadings illustrate the range of isotope values (min to max) from Ny-Ålesund and Samoylov Island, respectively, while the corresponding weekly median values are depicted as thicker blue and red lines. Dots overlaying the line graphs denote precipitation event samples collected during the MOSAiC year from Ny-Ålesund (blue) and Samoylov Island (red).

onward, a notable narrowing of the $\delta^{18}O$ difference between vapor and snow is observed (**Figure 1**). Hence, during periods of higher precipitation, the isotopic signals in snow and vapor become more closely aligned.

An extended version of these results, including the same analyses and figures incorporating an unpublished, higher-resolution dataset, is provided in the Appendix of the Supplementary Material.

3.3. Event-based precipitation isotopes

Figure 3a shows the drift track of PS in the Arctic during the MOSAiC expedition commencing at around 85°N, 128°E, and heading toward the Fram Strait. **Figure 3b** and **c** shows the isotopic compositions of $\delta^{18}O$ and *d-excess* of event-based precipitation, sampled at 2 continental stations: Samoylov Island and Ny-Ålesund. The former is located on the northern coast of Siberia, whereas the latter is located on Svalbard at the eastern entrance to the Fram Strait. This comparison is particularly valuable due to the absence of event-based precipitation sampling during the MOSAiC expedition. Long-term precipitation isotope data from Leroy-Dos Santos et al. (2020) for Ny-Ålesund and Bonne et al. (2020) for Samoylov Island are included to provide multiyear background information. The $\delta^{18}O$ values at Samoylov Island exhibit a clear seasonal cyclicity, as observed in both historical and MOSAiC-year records. During the winter months, there is a substantial decrease in $\delta^{18}O$ values from about −20‰ to −35‰. As temperatures increase in spring, the $\delta^{18}O$ values gradually rise to over −15‰. In contrast, Ny-Ålesund precipitation isotope data displays little fluctuation in $\delta^{18}O$ over the seasons, with $\delta^{18}O$ values stable around −10‰, which is due to fairly constant temperatures at this site throughout the year.

Both stations provide a wide range of *d-excess* values throughout the year. Samoylov Island's median *d-excess* values range around +10‰, with individual measurements down to −40‰. On the other hand, Ny-Ålesund exhibits larger variations, with median *d-excess* values fluctuating between around +5‰ in October and +25‰ in December, and occasionally reaching maxima as high as +35‰. During the period from May to September, both stations consistently show similar *d-excess* values that fall within the range of +10 to −10‰.

There are similarities and dissimilarities between monthly mean $\delta^{18}O_{snow}$ obtained during the MOSAiC expedition and precipitation samples recorded at both stations. Generally, the MOSAiC surface snow $\delta^{18}O$ data show a larger monthly variability than the precipitation data at both stations. The $\delta^{18}O_{snow}$ data show a seasonal cyclicity similar to that of Samoylov Island precipitation, not visible in the Ny-Ålesund multiannual dataset (**Figure 4a**). A distinct offset between the MOSAiC surface snow and Samoylov Island is observed in some months. For instance, in November and December 2019, the median $\delta^{18}O$ in precipitation at Samoylov Island is depleted by about 12‰ relative to that of surface snow. This offset decreases in January to −6‰, whereas from

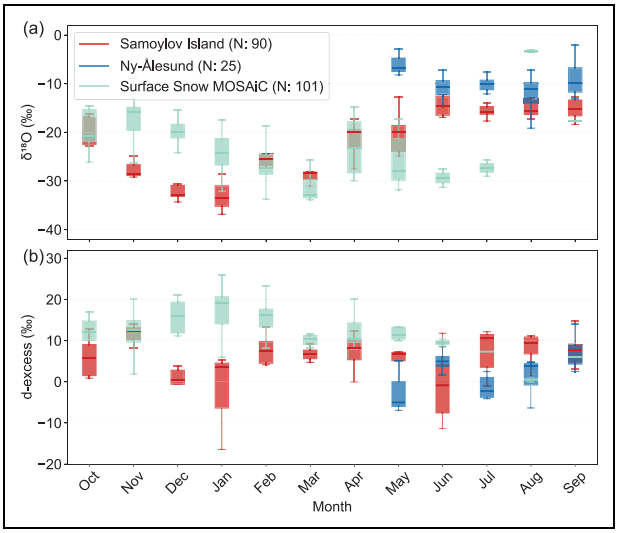

Figure 4. Monthly mean of isotope data from Arctic surface snow and continental precipitation (for the MOSAiC Year). Box plots provide a statistical summary of the monthly $\delta^{18}O$ (a) and *d-excess* (b) variability of surface snow compared to precipitation events at Samoylov Island and Ny-Ålesund stations, from the Pan-Arctic Precipitation Isotopes Network (PAPIN). In each boxplot, the medians are indicated by horizontal lines, the box boundaries represent the interquartile ranges, and the whiskers extend to the minimum and maximum values for each month.

February to April, the offset is positive from +2‰ to +4‰. Generally, the median MOSAiC $\delta^{18}O_{Snow}$ exhibits a negative offset (more depleted) compared to Ny-Ålesund data, and, except for August, consistently more depleted compared to Samoylov Island data, ranging from −2.6‰ (May) to −15‰ (August). The $\delta^{18}O$ interquartile ranges for surface snow and Samoylov Island overlap between January and September, whereas for Ny-Ålesund between June and August 2020, only.

The *d-excess* from MOSAiC surface snow shows significant month-to-month variability, ranging from slightly negative values in summer to over +20‰ during the winter months. The median values from October 2019 to May 2020 are higher than +10‰. We can confirm a clear seasonal *d-excess* cyclicity in surface snow, characterized by opposite trends between *d-excess* and $\delta^{18}O_{Snow}$ values (**Figure 4**). A noticeable offset between the median *d-excess* in surface snow and that of Samoylov Island is observed during winter, with Samoylov Island's *d-excess* being up to 15‰ lower (December, January) than that of surface snow. This bias gradually decreases toward zero by June (−2‰) and turns into a negative bias up to −9‰ (July, August) in the summer months. The seasonal *d-excess* cyclicity in Samoylov Island precipitation is less visible in the winter data. However, *d-excess* values of surface snow overlap within their interquartile ranges with that of Samoylov Island precipitation, from June to November.

The MOSAiC surface snow *d-excess* values often closely match those recorded at Ny-Ålesund. Ny-Ålesund *d-excess* values have a narrow distribution in summer, mostly ranging between −5‰ and +15‰. However, month May seems to be an outlier and the median *d-excess* of Ny-Ålesund is +17‰ lower than the MOSAiC snow median. Between June and September, Ny-Ålesund *d-excess* values overlap within their interquartile ranges with that of surface snow. The variance in Ny-Ålesund's *d-excess* values also increases during from December to April (**Figure 3c**).

4. Discussion

4.1. Snow profiles: Meteoric water origin and sea ice—snow interactions

The changes in the isotopic composition of snow profiles reflect the contribution of relatively depleted (in $\delta^{18}O$) meteoric water, and snow-sea ice dynamics characterized by a relative enrichment in $\delta^{18}O$ (**Figure 1a**, and described in Macfarlane et al., 2023b). During snow accumulation, a differentiation occurs within the snow cover: the upper layer becomes more depleted in $\delta^{18}O$ and has higher *d-excess* values. The lower layer becomes more enriched in $\delta^{18}O$ with lower than median *d-excess* values, which is caused by snow interacting with the sea ice surface through recrystallization of the sea ice surface (Macfarlane et al., 2023b). This enrichment in the snowpack is particularly noticeable when snow covers are thin due to the higher temperature gradients (**Figure 1a**). Through the analysis of discrete snow isotope measurements during an entire year (Macfarlane et al., 2023b), we found that snow on Arctic sea ice displays a distinct stratification, with depleted $\delta^{18}O$ and higher *d-excess* in the upper layer indicating meteoric snowfall contribution, and enriched $\delta^{18}O$ and lower *d-excess* values in the bottom layer due to interactions with underlying sea ice. To differentiate between meteoric and sea ice vapor sources in the Arctic is crucial for accurately modeling isotopic exchanges, especially in conditions of minimal snowfall. This new process understanding is critical throughout MOSAiC as it impacts the relationship between depleted atmospheric vapor and the more enriched winter snowpack. The contrast between fresh meteoric snow and snow influenced by sea ice diffusion from January to May leads to pronounced isotopic gradients (**Figure 1**). These results are important for refining modeling strategies used in regional and global atmosphere models with isotope diagnostics (Brunello et al., 2023).

Between June and September 2020, as temperatures approach 0°C, the initial thaw causes the formation of melt ponds on the sea ice. These ponds deepen until they penetrate through the sea ice, facilitating freshwater mixing with seawater (Nomura et al., 2023). The early stages of melting are characterized by a shallow and wet layer of snow that covers the sea ice, influenced by 2 distinct isotopic values. At first, meltwater percolation starts from the surface, resulting in the preferential melting of the upper snow layers. During this process, meltwater percolates through the snowpack, diminishing the variation in its isotopic composition (Moran and Marshall, 2009). This meltwater movement results in a more uniform isotopic composition across different layers of snow (**Figure 1**), demonstrating how seasonal temperature increases

induce melt events that can enrich the snowpack in heavier isotopes.

4.2. The linkage between MOSAiC surface snow and atmospheric water vapor

The seasonal transition throughout the MOSAiC-year highlights (1) the relationship between the intensity and intermittency of precipitation and (2) the transfer of isotopic values between the atmospheric water vapor and surface snow.

October to December 2019 is the period when the largest mismatch between snow and vapor $\delta^{18}O$ values occurs (**Figure 2**). This offset can be attributed to 2 primary factors. The first point is that the vapor time series represents real-time conditions, while the snow cover corresponds to one or more past precipitation events. The time between the initial precipitation and sampling could range from a few days to several weeks. Hence, the snow might carry an inherited isotopic values from older winter snow, as seen in other snow studies from Greenland (Zuhr et al., 2021), which is not necessarily related to the vapor at a given time. Second, the influx of warm air during autumn 2019 (warm air intrusions, **Figure 5**) often brought additional moisture and heat to the region, generally characterized by isotopically enriched Atlantic moisture (Brunello et al., 2023), which would in general lead to higher $\delta^{18}O$ values in snow. Similar values and a relatively close range of *d-excess* in snow and vapor during this period (Figure S3) could be either interpreted as an indicator for similar moisture sources for snow and vapor, or indicate little influence of secondary processes taking place after the deposition of snow.

From January and May 2020, a phase of discrepancy between $\delta^{18}O_{Snow}$ and $\delta^{18}O_{Vapor}$ (**Figure 2**) as well as between *d-excess* in vapor and snow is observed (Figure S3). During this period, there are substantial differences between the $\delta^{18}O_{Snow}$ and $\delta^{18}O_{Vapor}$, of up to 24‰ (**Figure 2**). This period corresponds to the most extreme cold and dry period of winter, when PS was initially located in the Siberian sector of the Arctic Ocean, then drifting into the Atlantic sector (**Figure 3a**) in March 2020. These offsets and the weather conditions favorable for sublimation (negative heat flux, **Figure 5**) may imply that kinetic isotopic fractionation in the form of sublimation has contributed to these deviations between vapor and deposited snow, which has undergone sublimation after precipitation.

The observed offsets between $\delta^{18}O_{Snow}$ and $\delta^{18}O_{Vapor}$, as well as related *d-excess* values, allow for the categorization of the development of the Arctic snow cover into 3 distinct stages: (1) an early winter phase, with a clear offset in $\delta^{18}O$, but not in *d-excess* (October to December 2019), (2) the late winter phase characterized by extremely cold temperatures and low humidity, where the disequilibrium between vapor and snow is most pronounced (January to May 2020), (3) summer where all the snow has melted on level ice and a surface scattering layer has appeared (June and August 2020). Furthermore, the offset experiences another rise in September 2020 (leg 5) when the PS travels back to the central Arctic (87°N), where the PS passed in February 2020, half a year before. This marks the end of the annual cycle, essentially reverting to the autumn situation and closing the seasonal cycle observed during the MOSAiC year.

4.3. Impacts of precipitation amounts and air temperature on snow-vapor isotopic correlations

A weak correlation between the $\delta^{18}O$ values of snow and vapor reflects the theoretical concept of equilibrium fractionation ($R^2 = 0.10$, shown in the trendline in **Figure 6b**). This correlation strengthens slightly during major precipitation events (>2 mm/day, $R^2 = 0.28$), outlined with larger markers in **Figure 6b**, likely due to higher humidity, faster isotopic transfer, shorter atmospheric residence times, and more equilibrium fractionation is expected. Hence, the amount of precipitation impacts $\delta^{18}O$ because of the addition of meteoric water, especially during the summer months in the Arctic. The correlations between $\delta^{18}O_{Snow}$ and $\delta^{18}O_{Vapor}$ remain low in winter, suggesting the persistent, overlaying impact of postdepositional processes decoupling vapor and snow, outlined in the previous section.

The seasonal dynamics of $\delta^{18}O$ in snow and vapor reveal contrasting patterns with air temperature. $\delta^{18}O_{Vapor}$ strongly correlates with temperature ($R^2 = 0.73$; **Figure 7a**), aligning with theoretical expectations (Dansgaard, 1964). In contrast, $\delta^{18}O_{Snow}$ shows a weaker correlation ($R^2 = 0.10$), reflecting the influence of postdepositional processes (Ala-aho et al., 2021). These modifications begin immediately after precipitation, altering snow isotopic composition through sublimation and vapor deposition during snow metamorphism (Macfarlane et al., 2023b), which occur on sub-daily timescales (Ritter et al., 2016; Wahl et al., 2021). Limited sampling intensity in this study does not capture such rapid changes, particularly during precipitation-free periods, when sublimation enriches the snow in heavier isotopes (Wahl et al., 2022).

Throughout the expedition, $\delta^{18}O$ correlations in snow and vapor with air temperature revealed distinct seasonal patterns (**Figure 7**). From October to December 2019, $\delta^{18}O_{Vapor}$ showed a strong temperature sensitivity (slope: 0.69‰/°C, $R^2 = 0.63$), while $\delta^{18}O_{Snow}$ remained unaffected. During the winter months (January to May 2020), $\delta^{18}O_{Snow}$ exhibited a slight temperature response (slope: 0.28‰/°C, $R^2 = 0.17$) but varied widely under similar conditions, suggesting a complex interplay of factors influencing the snow isotopic composition.

4.4. Comparison of MOSAiC surface snow with continental precipitation

The transit of the PS between Samoylov Island (Northern Siberia) and Ny-Ålesund (Svalbard) highlights differences in isotopic values at the MOSAiC expedition starting and endpoints. Samoylov Island exhibits a distinct annual $\delta^{18}O$ cycle, reflecting a wide temperature range (−45°C to +25°C) typical of pan-Arctic continental climates (Halvorsen et al., 2015; Akers et al., 2020; Mellat et al., 2021), with pronounced winter minima and summer maxima, similar to patterns observed in Alaska (Klein and Welker, 2016; Bailey et al., 2019). In contrast, Ny-Ålesund shows

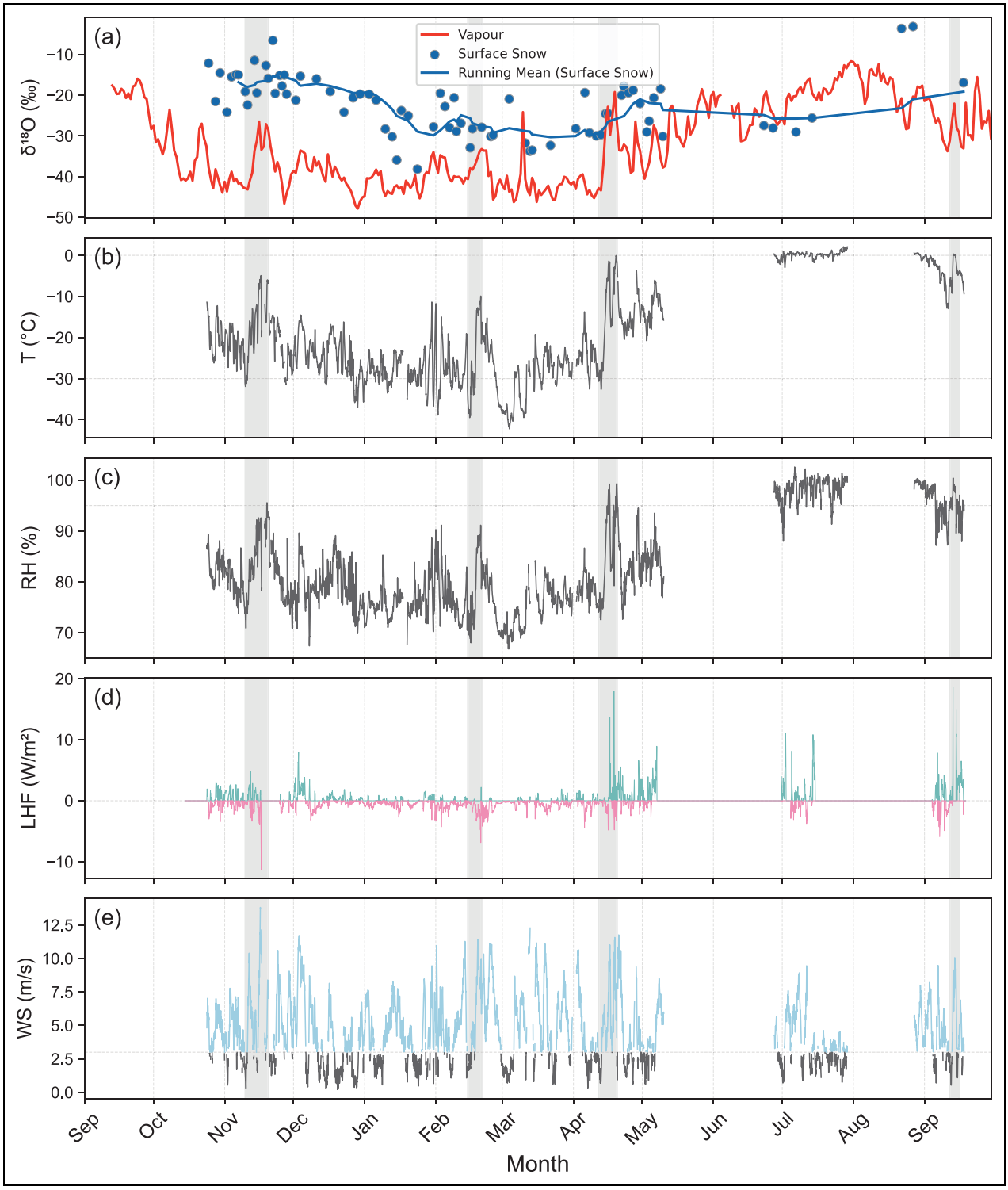

Figure 5. Seasonal fluctuations in meteorological and isotopic data captured during the MOSAiC expedition. (a) Depicts daily average $\delta^{18}O$ isotopic ratios in surface snow (blue dots) and the daily average vapor (red line). (b) Illustrates air temperature at 2 m above ground level (T, °C) on an hourly basis, and (c) the hourly relative humidity against saturation over water (RH, %). (d) shows the latent heat flux (LHF, W/m^2) measured hourly. Positive LHF values suggest evaporative loss and negative values deposition, revealing intermittent events across the seasons. The bottom graph (e) shows the hourly wind speed (WS, m/s), applying a 3 m/s threshold to denote significant snow movement as suggested by Wagner et al. (2022); wind speeds surpassing this threshold are highlighted in light blue. The period of warm air intrusion event identified during the expedition (Rinke et al., 2021) is shown as gray bars on all panels. The meteorological data are extracted from the meteorological tower (MET) tower observations during MOSAiC expedition (Cox et al., 2023).

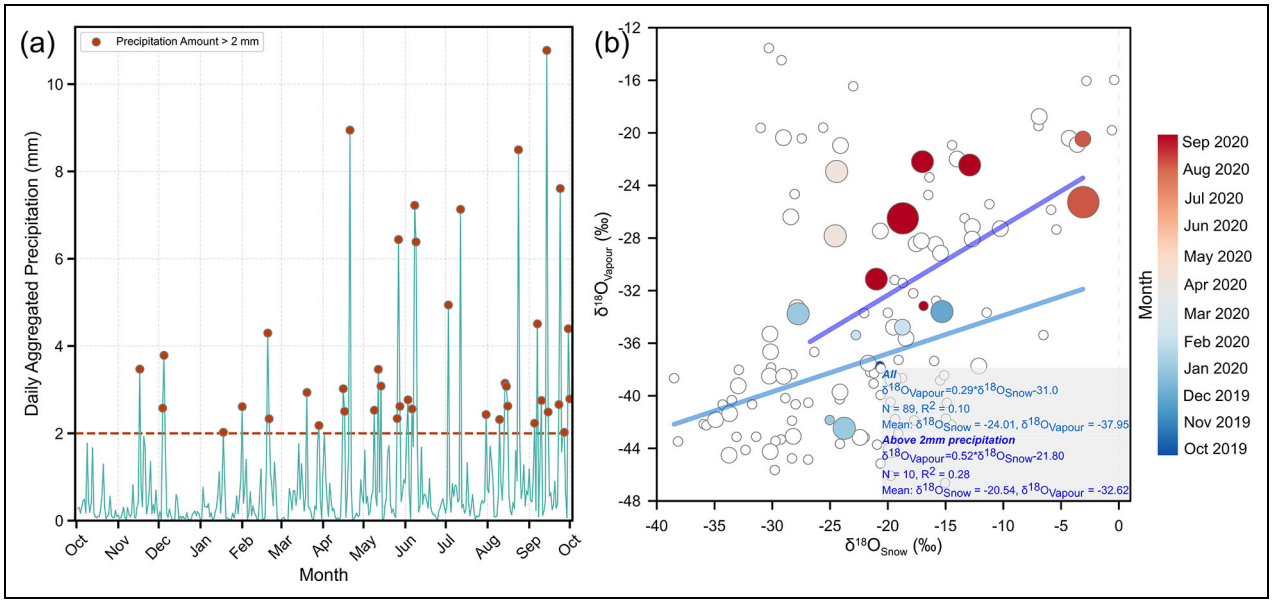

Figure 6. Comparative analysis of precipitation and isotopic composition. (a) The left panel displays the daily aggregated precipitation over a year (reanalysis data from ERA5), with the horizontal dashed line indicating a threshold of 2 mm for significant precipitation events, highlighted by red circles. (b) The right panel presents a scatter plot correlating the $\delta^{18}O$ values of snow ($\delta^{18}O_{Snow}$) with those of vapor ($\delta^{18}O_{Vapor}$). Each point represents a measurement, with the color gradient reflecting the progression of months from October 2019 to September 2020. Two distinct regression lines are shown: the light blue line represents all surface snow samples ($N = 125$), while the dark blue line corresponds to surface snow samples collected within 5 days after precipitation events of more than 2 mm ($N = 26$). The corresponding regression equations, coefficient of determination (R^2), and mean $\delta^{18}O$ values for snow and vapor are provided for both datasets. The size of each point is proportional to the amount of precipitation on the corresponding day.

moderate $\delta^{18}O$ seasonality due to its proximity to the Atlantic Ocean, the primary moisture source, and a narrower temperature range (−12°C to +6°C). This limited seasonality at Ny-Ålesund is driven by isotopically enriched Atlantic moisture throughout the year (Boisvert et al., 2023). The colder conditions at Samoylov Island consistently result in lower (depleted) $\delta^{18}O$ values compared to Ny-Ålesund.

For *d-excess*, Ny-Ålesund shows higher variability than Samoylov Island. In summer, reduced variability in $\delta^{18}O$ and *d-excess* at Samoylov Island indicates shared moisture sources with similar evaporation conditions, a pattern absent at Ny-Ålesund. Comparing MOSAiC precipitation data to long-term climatology (Bonne et al., 2020; Leroy-Dos Santos et al., 2020) shows that Samoylov $\delta^{18}O$ and *d-excess* values align with historical medians, with November 2019 showing lower $\delta^{18}O$ values, potentially indicating an earlier onset of colder conditions. Similarly, Ny-Ålesund precipitation $\delta^{18}O$ and *d-excess* values during May–September 2020 align with historical trends, suggesting consistent summer humidity and temperature conditions.

The MOSAiC snow isotope dataset reveals a delayed response in snowpack $\delta^{18}O$ values compared to Samoylov Island precipitation, with a 2-month lag in reaching the winter minimum (March 2020). This lag suggests a complex relationship between precipitation and snowpack integration, indicating different winter moisture sources or precipitation patterns between Samoylov Island and the central Arctic Ocean, potentially influenced by the Barents and Kara seas open water (Bailey et al., 2021). During October–November 2019, *d-excess* values for Samoylov precipitation and MOSAiC snow are similar (approximately 10‰, **Figure 4b**) but diverge as the PS moves further from Samoylov Island. This divergence reflects shifting moisture sources, with Atlantic moisture dominating by June–July, lowering *d-excess* values across Samoylov Island, Ny-Ålesund, and MOSAiC snow (Mellat et al., 2021).

4.5. Depositional and postdepositional processes imprint on surface snow isotopes

The variations in the $\delta^{18}O_{Vapor}$ during warm air intrusions, like those that occurred in November 2019 and April 2020 (Rinke et al., 2021), show that the isotopic composition of water vapor responds to changes in air temperature and RH at the evaporative sites (Brunello et al., 2023). However, $\delta^{18}O_{Snow}$ does not correlate to atmospheric conditions. Although warm air brought into the Arctic is expected to contribute precipitation to the snow profiles, $\delta^{18}O_{Snow}$ does not show a clear impact from such additions (**Figure 5**), suggesting that deposited snow undergoes isotope alteration and postdepositional processes such as wind redistribution might impact its isotopic values.

Between December 2019 and March 2020, a gradual depletion in $\delta^{18}O_{Snow}$ was observed (**Figure 5a**), presumably driven by the concurrent slight decrease in air

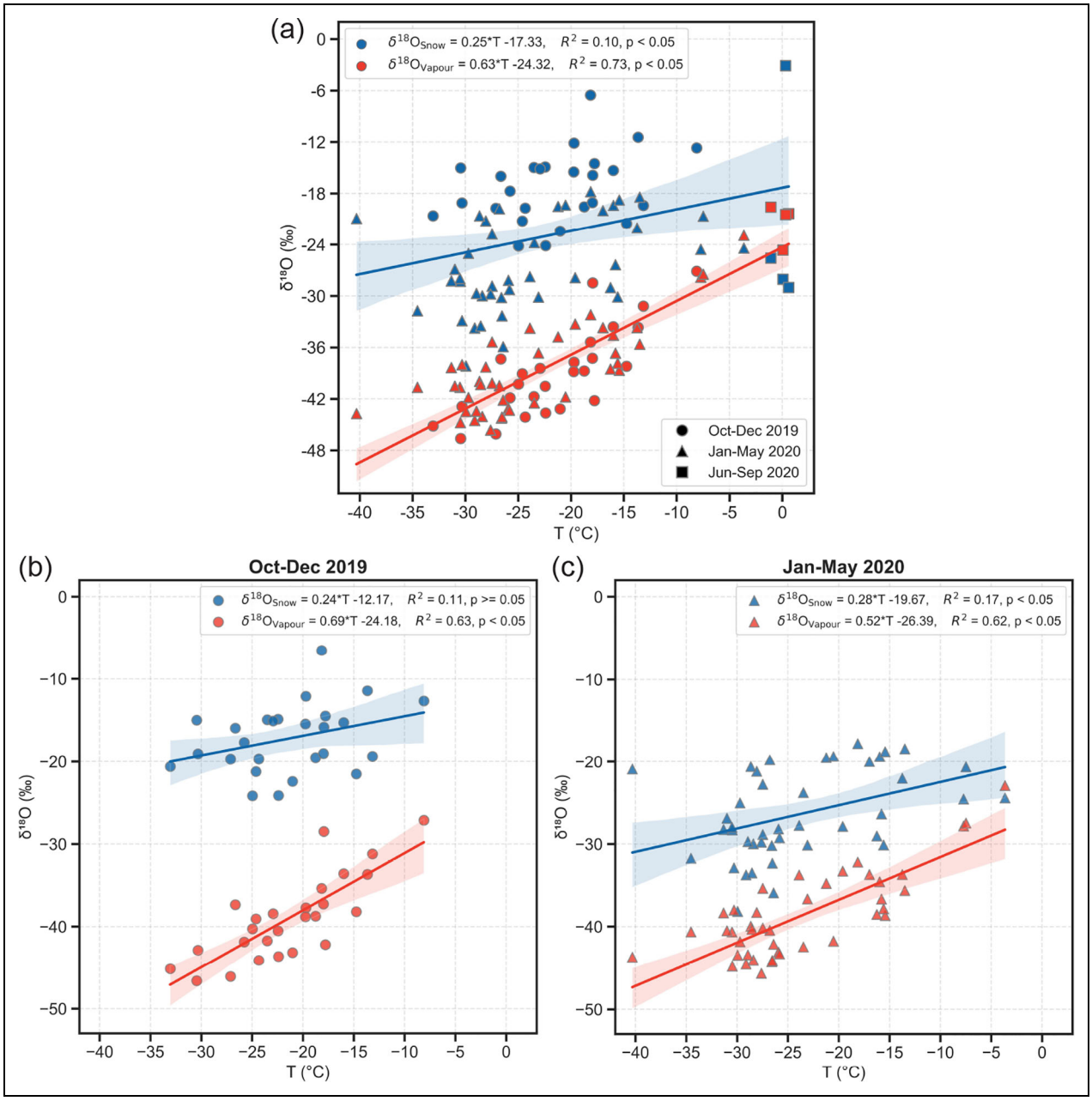

Figure 7. Temperature dependence of isotopic ratios in snow and vapor. The figure illustrates the relationship between air temperature (T (°C)) and the mean daily $\delta^{18}O$ surface snow ($\delta^{18}O_{Snow}$) and vapor ($\delta^{18}O_{Vapor}$) during (a) MOSAiC expedition from October 2019 to September 2020. Data points are differentiated by the period of the year they represent: circles for October to December 2019, triangles for January to May 2020, and squares for June to September 2020. (b) Represents data from October to December 2019, and (c) from January to May 2020. Each panel illustrates the corresponding linear regression analyses for $\delta^{18}O_{Snow}$ (blue lines) and $\delta^{18}O_{Vapor}$ (red lines) within each period. The shaded areas around each regression line indicate the 95% confidence intervals.

temperature levels (**Figure 5b**). However, relatively constant cold conditions during this period let us expect that surface sublimation may have contributed to this trend. This is supported by the mostly (72% of the total period) negative LHF observed during this time (**Figure 5d**). Sublimation introduces another level of complexity to interpreting the deposited snow isotopic values. The porosity of snow allows for significant sublimation, leading to an influence on both the $\delta^{18}O$ and *d-excess* (Casado et al., 2021). It has been found that the longer residence time of snow on the surface, which facilitates isotopic homogeneity of individual ice grains through solid-phase diffusion, may contribute to the enrichment of snow in $\delta^{18}O$ and increased *d-excess* (Zuhr et al., 2023). In contrast with the previous assumptions of layer-by-layer sublimation without isotopic fractionation (Ambach et al., 1968; Dansgaard et al., 1973), sublimation may play a key control in the isotopic composition of snow in polar regions.

High wind velocities and sea ice aerodynamic properties cause significant snow redistribution, with large amounts of snow mass lost through sublimation when

snow is in the air (Wagner et al., 2022). Moreover, the flattening of the snow surface and reduction in surface roughness due to wind-driven erosion can influence sublimation rates and the efficiency of vapor exchange between the snowpack and the atmosphere (Zuhr et al., 2021). During winter, there was a significant redistribution of snow, which occurred 67% of the time (WS > 3 m/s, **Figure 5e**) (Wagner et al., 2022). The mixing and redistribution of snow on sea ice likely homogenized the $\delta^{18}O_{Snow}$ signal on the sea ice. This process could lead to a shift toward enrichment in the top layer of the snow, as snow with lower $\delta^{18}O$ values from meteoric sources was spread across the surface, likely also responsible for the low $\delta^{18}O$-air temperature correlation coefficients in surface snow (**Figure 7**). This mixing effect is also apparent in the snow profiles collected from the ridges (Figure S4), where the upper layers exhibit a homogeneous $\delta^{18}O$ signal, in contrast to the flat ice samples (**Figure 1a**).

June and July 2020 experienced the highest air temperatures throughout the MOSAiC expedition and near-saturation levels of humidity. Although conditions for water vapor sublimation occurred less frequently, representing just 12% of times (LHF < 0 W/m^2, **Figure 5d**). Despite this, the snow on the sea ice was predominantly identified as wet, comprising a mix of slush, making its redistribution less probable. Therefore, we can conclude that snow redistribution plays a more significant role in altering the isotopic value of surface snow during winter than in summer. Over this warmer time, it is noteworthy that half of the collected samples displayed a $\delta^{18}O_{Snow}$ influenced by the real-time meteorological conditions (i.e., higher air temperatures), resulting in more enriched values ranging from −3‰ to −15‰. The remaining half of the samples collected from the ridges exhibited a signal more typical of meteoric winter snow, with values ranging from −20‰ to −30‰ (**Figure 5a**).

The isotopic composition of snow can undergo significant changes due to partial melting, which is particularly relevant when temperatures are close to 0°C. Due to disequilibrium fractionation during melting, lighter oxygen isotopes preferentially enter the liquid phase, thus leading to higher $\delta^{18}O$ values in the remaining snow (Friedman et al., 1991; Clark and Fritz, 2013; Beria et al., 2018). This leads to an isotopic enrichment of $\delta^{18}O_{Snow}$, when initial meltwaters drain into melt ponds, leads, and the ocean (Nomura et al., 2023). By August and September 2020, melting processes cause a relatively $\delta^{18}O$-enriched, homogenized snowpack. This phase reflects the interplay between melting dynamics and isotopic composition and is responsible for alterations of isotopes at the Arctic snow and sea ice interface in this melting period.

In summary, postdepositional processes substantially modify the initial depositional isotopic values, as indicated by the low correlation between snow isotopes with both vapor isotopes and air temperature. The influence of these postdepositional processes varies seasonally. Wind drift, which occurs consistently throughout the year, preferentially removes dry snow, resulting in isotope homogenization, particularly on ridges. A significant postdepositional effect involves the interaction between snow and the sea ice surface, where high-temperature gradients in winter induce upward water vapor diffusion, thereby modifying the isotope profile from below (Macfarlane et al., 2023b). This recrystallized sea ice contributes to the snowpack and enriches the snow crystals, creating snow with an enriched $\delta^{18}O$ signal similar to that of the underlying sea ice. Although these processes are challenging to distinguish and quantify, a wintertime comparison indicates that the net effect of all postdepositional processes leads to an overall shift of about −15‰ in the MOSAiC $\delta^{18}O_{Snow}$ samples relative to Samoylov Island's winter time series. This difference may reflect increased snow metamorphism, stronger wind redistribution, or other environment-specific factors at the MOSAiC site compared to Samoylov Island.

5. Conclusions

This study addresses the link between the deposition and postdepositional processes that impact the stable water isotope values in snow on Arctic sea ice, using a dataset from the MOSAiC expedition. The analysis suggests that the isotopic composition of Arctic snow is only partially controlled by depositional processes and instead is heavily influenced by postdepositional processes, in particular in the winter. The use of continuous vapor isotope measurements alongside discrete snow samples allows for a better understanding of the snow–atmosphere interaction and the associated processes affecting isotopic values in the Arctic snow.

Our study identified 3 main phases in the isotopic composition of Arctic snow cover throughout the year. Each phase is characterized by distinctive connections between the $\delta^{18}O$ values and *d-excess* of snow and vapor, demonstrating the dynamic nature of Arctic atmosphere–snow interactions:

1. Autumn and early winter are characterized by a $\delta^{18}O$ offset with relatively enriched snow, and consistently positive *d-excess* in snow, reflecting a lag in the snow isotopic adaptation to precipitation and the impact of isotopically enriched Atlantic air. During this phase, $\delta^{18}O_{Snow}$ remains relatively unaffected by air temperature shifts, whereas $\delta^{18}O_{Vapor}$ shows expected temperature correlations, highlighting the significant role of postdepositional processes on the sea ice in altering $\delta^{18}O_{Snow}$.
2. Cold months of winter are marked by a pronounced decoupling between vapor and snow under low humidity. During the winter, colder temperatures generally caused fresh snow to be more depleted in $\delta^{18}O$. However, due to sublimation, wind redistribution, and the associated fractionation processes, a wide range of $\delta^{18}O_{Snow}$ values was observed due to the enrichment associated with these postdepositional processes introducing substantial variability in the values measured.
3. Transitioning into spring and summer, the gap between snow and vapor isotopic values narrow, suggesting a shift toward equilibrium fractionation.

This is accompanied by a noticeable link between warming temperatures, increased humidity, and a pronounced $\delta^{18}O_{Vapor}$ response. Surface snow differentiates into 2 categories: ridge snow, tended to mirror winter's depleted $\delta^{18}O$ values, and snow on flat ice, exhibiting enriched $\delta^{18}O$ due to melt-freeze cycles and sea ice–snow interaction. Additionally, this period is supposed to witness intensified sublimation, leading to a further increase in $\delta^{18}O$ in surface snow on flat ice.

Future research should aim to improve the temporal resolution of snow on ice isotope measurements to capture isotopic variability more precisely. There is a pressing need for detailed, short-interval measurements of snow isotopes and their physical properties, ideally hourly to daily. A higher temporal resolution of measurements would allow future research to better investigate sublimation, a phase transition known to modify the isotopes of surface snow. Additionally, deploying continuous vapor isotope measurements close to the snow surface could provide a more detailed understanding of the local versus advective moisture contributions to the snow isotopic composition. These methodological improvements could significantly refine our understanding of the snow–atmosphere interactions and their representation in climate models.

Data accessibility statement

All data in this manuscript are publicly available from online repositories. The data can be found under the following references:

- Stable water isotopes of snow during MOSAiC expedition (Mellat et al., 2022).
- Snow pit raw data collected during the MOSAiC expedition (Macfarlane et al., 2022).
- Continuous near-surface atmospheric water vapor isotopic composition from Polarstern cruise PS122-1:5 (Brunello et al., 2022a; Brunello et al., 2022b; Brunello et al., 2022c; Brunello et al., 2022d; Brunello et al., 2022e).

Supplemental files

The supplemental files for this article can be found as follows:

Figures S1–S4. Table S1. Appendix Figures 1–8. PDF

Acknowledgments

We would like to express our gratitude to the International Multidisciplinary Drifting Observatory for the Study of the Arctic Climate (MOSAiC) with the tag MOSAiC20192020 for providing the opportunity to conduct this research and for producing the data used in this report. Specifically, we would like to thank all people who were involved in this expedition of the research vessel Polarstern (Knust, 2017) and helped to collect the samples during MOSAiC in the 2019–2020 project (Project ID: AWI_PS122_00) (Nixdorf et al., 2021). We extend our sincere appreciation to all the persons involved in the expedition of the RV Polarstern during MOSAiC in 2019–2020 (AWI_PS122_00). We also thank Mikaela Weiner and Andreas Marent for isotope analyses ($\delta^{18}O$, $\delta^{2}H$) of the samples in the ISOLAB Facility at AWI in Potsdam.

Funding

MM, CFB, MW, and HM are grateful for the support provided by the German Federal Ministry of Education and Research (project MOSAiC-CiASOM, grant number 03FO869A). MS, ARM, and RD received funding from the Swiss Polar Institute (SPI reference DIRCR-2018-003) Funder ID: http://dx.doi.org/10.13039/501100015594, European Union's Horizon 2020 research and innovation program projects ARICE (grant 730965) for berth fees associated with the participation of the DEARice project, and WSL Institute for Snow and Avalanche Research SLF. WSL_201812N1678. Funder ID: http://dx.doi.org/10.13039/501100015742. ARM received funding from the Swiss National Science Foundation (SNSF) project number P500PN_217845. JMW was supported in part by NSF AON award 1852614 for Arctic water isotope cycle processes and patterns in the Central Arctic during an International Arctic Drift Expedition (MOSAiC); and by his UArctic Research Chairship. K-RM was supported by Kone Foundation, Research Council of Finland project #347662, and The Land and Water Technology Foundation (MVTT). SA was supported by the Alfred-Wegener-Institut, Helmholtz-Zentrum für Polar- und Meeresforschung, the University of Hamburg, the German Research Foundation's (DFG) projects fAntasie (AR1236/3-1) and SnowCast (AR1236/1-1) within its priority program "Antarctic Research with comparative investigations in the Arctic ice areas" (SPP1158), and the DFG Emmy Noether Programme project SNOWflAke (project number 493362232).

Competing interests

All authors declare that they have no competing interests.

Author contributions

MM, ARM, HM, CFB, MW, and MS contributed to the conception and design. The acquisition of data was carried out by MM, ARM, HM, CFB, MW, MS, RD, SA, K-RM, and JMW. Analysis and interpretation of the data were performed by MM, ARM, CFB, HM, MW, MS, JMW, and RD. Drafting and revising the article was done by MM, ARM, CFB, MW, MS, RD, SA, K-RM, JMW, and HM.

References

Aemisegger, F. 2018. On the link between the North Atlantic storm track and precipitation deuterium excess in Reykjavik. *Atmospheric Science Letters* **19**(12): e865. DOI: https://doi.org/10.1002/asl.865.

Akers, PD, **Kopec, BG**, **Mattingly, KS**, **Klein, ES**, **Causey, D**, **Welker, JM.** 2020. Baffin Bay sea ice extent and synoptic moisture transport drive water vapor isotope ($\delta^{18}O$, $\delta^{2}H$, and deuterium excess) variability in coastal northwest Greenland. *Atmospheric Chemistry and Physics* **20**(22): 13929–13955. DOI: https://doi.org/10.5194/acp-20-13929-2020.

Ala-aho, P, **Welker, JM**, **Bailey, H**, **Højlund Pedersen, S**, **Kopec, B**, **Klein, E**, **Mellat, M**, **Mustonen, K-R**, **Noor, K**, **Marttila, H.** 2021. Arctic snow isotope hydrology: A comparative snow-water vapor study. *Atmosphere* **12**(2): 150. DOI: https://doi.org/10.3390/atmos12020150.

Ambach, W, **Dansgaard, W**, **Eisner, H**, **Moller, J.** 1968. The altitude effect on the isotopic composition of precipitation and glacier ice in the Alps. *Tellus A: Dynamic Meteorology and Oceanography* **20**(4): 595–600. DOI: https://doi.org/10.3402/tellusa.v20i4.10040.

Bailey, H, **Hubbard, A**, **Klein, ES**, **Mustonen, K-R**, **Akers, PD**, **Marttila, H**, **Welker, JM.** 2021. Arctic sea-ice loss fuels extreme European snowfall. *Nature Geoscience* **14**(5): 283–288. DOI: https://doi.org/10.1038/s41561-021-00719-y.

Bailey, HL, **Klein, ES**, **Welker, JM.** 2019. Synoptic and mesoscale mechanisms drive winter precipitation $\delta^{18}O/\delta^{2}H$ in south-central Alaska. *Journal of Geophysical Research: Atmospheres* **124**(7): 4252–4266. DOI: https://doi.org/10.1029/2018jd030050.

Beria, H, **Larsen, JR**, **Ceperley, NC**, **Michelon, A**, **Vennemann, T**, **Schaefli, B.** 2018. Understanding snow hydrological processes through the lens of stable water isotopes. *WIREs Water* **5**(6): e1311. DOI: https://doi.org/10.1002/wat2.1311.

Boisvert, LN, **Parker, C**, **Valkonen, E.** 2023. A warmer and wetter Arctic: Insights from a 20-years AIRS record. *Journal of Geophysical Research: Atmospheres* **128**(20): e2023JD038793. DOI: https://doi.org/10.1029/2023jd038793.

Bonne, J-L, **Meyer, H**, **Behrens, M**, **Boike, J**, **Kipfstuhl, S**, **Rabe, B**, **Schmidt, T**, **Schönicke, L**, **Steen-Larsen, HC**, **Werner, M.** 2020. Moisture origin as a driver of temporal variabilities of the water vapour isotopic composition in the Lena River Delta, Siberia. *Atmospheric Chemistry and Physics* **20**(17): 10493–10511. DOI: https://doi.org/10.5194/acp-20-10493-2020.

Brunello, CF, **Gebhardt, F**, **Rinke, A**, **Dütsch, M**, **Bucci, S**, **Meyer, H**, **Mellat, M**, **Werner, M.** 2024. Moisture transformation in warm air intrusions into the Arctic: Process attribution with stable water isotopes. *Geophysical Research Letters* **51**(21): e2024GL111013. DOI: https://doi.org/10.1029/2024gl111013.

Brunello, CF, **Meyer, H**, **Mellat, M**, **Casado, M**, **Bucci, S**, **Dütsch, M**, **Werner, M.** 2023. Contrasting seasonal isotopic signatures of near-surface atmospheric water vapor in the central Arctic during the MOSAiC campaign. *Journal of Geophysical Research: Atmospheres* **128**(24): e2022JD038400. DOI: https://doi.org/10.1029/2022jd038400.

Brunello, CF, **Werner, M**, **Meyer, H**, **Mellat, M**, **Bonne, J-L.** 2022a. Continuous near-surface atmospheric water vapour isotopic composition from Polarstern cruise PS122-1 (MOSAiC) [dataset]. PANGAEA. DOI: https://doi.org/10.1594/PANGAEA.951424.

Brunello, CF, **Werner, M**, **Meyer, H**, **Mellat, M**, **Bonne, J-L.** 2022b. Continuous near-surface atmospheric water vapour isotopic composition from Polarstern cruise PS122-2 (MOSAiC) [dataset]. PANGAEA. DOI: https://doi.org/10.1594/PANGAEA.951446.

Brunello, CF, **Werner, M**, **Meyer, H**, **Mellat, M**, **Bonne, J-L.** 2022c. Continuous near-surface atmospheric water vapour isotopic composition from Polarstern cruise PS122-3 (MOSAiC) [dataset]. PANGAEA. DOI: https://doi.org/10.1594/PANGAEA.951447.

Brunello, CF, **Werner, M**, **Meyer, H**, **Mellat, M**, **Bonne, J-L.** 2022d. Continuous near-surface atmospheric water vapour isotopic composition from Polarstern cruise PS122-4 (MOSAiC) [dataset]. PANGAEA. DOI: https://doi.org/10.1594/PANGAEA.951448.

Brunello, CF, **Werner, M**, **Meyer, H**, **Mellat, M**, **Bonne, J-L.** 2022e. Continuous near-surface atmospheric water vapour isotopic composition from Polarstern cruise PS122-5 (MOSAiC) [dataset]. PANGAEA. DOI: https://doi.org/10.1594/PANGAEA.951449.

Casado, M, **Landais, A**, **Picard, G**, **Arnaud, L**, **Dreossi, G**, **Stenni, B**, **Prié, F.** 2021. Water isotopic signature of surface snow metamorphism in Antarctica. *Geophysical Research Letters* **48**(17): e2021GL093382. DOI: https://doi.org/10.1029/2021gl093382.

Casado, M, **Landais, A**, **Picard, G**, **Münch, T**, **Laepple, T**, **Stenni, B**, **Dreossi, G**, **Ekaykin, A**, **Arnaud, L**, **Genthon, C**, **Touzeau, A**, **Masson-Delmotte, V**, **Jouzel, J.** 2018. Archival processes of the water stable isotope signal in East Antarctic ice cores. *The Cryosphere* **12**(5): 1745–1766. DOI: https://doi.org/10.5194/tc-12-1745-2018.

Clark, ID, **Fritz, P.** 2013. *Environmental isotopes in hydrogeology*. Boca Raton, FL: CRC Press. DOI: https://doi.org/10.1201/9781482242911.

Colbeck, SC. 1980. Thermodynamics of snow metamorphism due to variations in curvature. *Journal of Glaciology* **26**(94): 291–301. DOI: https://doi.org/10.3189/S0022143000010832.

Cox, C, **Gallagher, M**, **Shupe, M**, **Persson, O**, **Blomquist, B**, **Grachev, A**, **Riihimaki, L**, **Kutchenreiter, M**, **Morris, V**, **Solomon, A.** 2023. Met City meteorological and surface flux measurements (Level 3 Final), Multidisciplinary Drifting Observatory for the Study of Arctic Climate (MOSAiC), central Arctic, October 2019-September 2020. Arctic Data Center. DOI: https://doi.org/10.18739/A2PV6B83F.

Craig, H. 1961. Isotopic variations in meteoric waters. *Science* **133**(3465): 1702–1703. DOI: https://doi.org/10.1126/science.133.3465.1702.

Dadic, R, **Schneebeli, M**, **Bertler, NAN**, **Schwikowski, M**, **Matzl, M.** 2015. Extreme snow metamorphism in the Allan Hills, Antarctica, as an analogue for glacial conditions with implications for stable isotope composition. *Journal of Glaciology* **61**(230): 1171–1182. DOI: https://doi.org/10.3189/2015JoG15J027.

Dansgaard, W. 1964. Stable isotopes in precipitation. *Tellus A: Dynamic Meteorology and Oceanography* **16**(4): 436–468. DOI: https://doi.org/10.3402/tellusa.v16i4.8993.

Dansgaard, W, **Johnsen, SJ**, **Clausen, HB**, **Gundestrup, N.** 1973. Stable isotope glaciology. *Meddelelser Om*

Grønland **197**(2): 1–53. DOI: https://doi.org/10.7146/mog.v197.147754.

Feldl, N, **Po-Chedley, S**, **Singh, HKA**, **Hay, S**, **Kushner, PJ.** 2020. Sea ice and atmospheric circulation shape the high-latitude lapse rate feedback. *npj Climate and Atmospheric Science* **3**(1): 41. DOI: https://doi.org/10.1038/s41612-020-00146-7.

Friedman, I, **Benson, C**, **Gleason, J.** 1991. Isotopic changes during snow metamorphism, in Taylor, HP, O'Neil, JR, Kaplan, IR eds., *Stable isotope geochemistry: A tribute to Samuel Epstein*. San Antonio, TX: The Geochemical Society: 211–221.

Geerts, B, **Giangrande, SE**, **McFarquhar, GM**, **Xue, L**, **Abel, SJ**, **Comstock, JM**, **Crewell, S**, **Demott, PJ**, **Ebell, K**, **Field, P**, **Hill, TCJ**, **Hunzinger, A**, **Jensen, MP**, **Johnson, KL**, **Juliano, TW**, **Kollias, P**, **Kosovic, B**, **Lackner, C**, **Luke, E**, **Lüpkes, C**, **Matthews, AA**, **Neggers, R**, **Ovchinnikov, M**, **Powers, H**, **Shupe, MD**, **Spengler, T**, **Swanson, BE**, **Tjernström, M**, **Theisen, AK**, **Wales, NA**, **Wang, Y**, **Wendisch, M**, **Wu, P.** 2022. The COMBLE campaign: A study of marine boundary layer clouds in Arctic cold-air outbreaks. *Bulletin of the American Meteorological Society* **103**(5): E1371–E1389. DOI: https://doi.org/10.1175/bams-d-21-0044.1.

Gong, X, **Zhang, J**, **Croft, B**, **Yang, X**, **Frey, MM**, **Bergner, N**, **Chang, RY-W**, **Creamean, JM**, **Kuang, C**, **Martin, RV**, **Ranjithkumar, A**, **Sedlacek, AJ**, **Uin, J**, **Willmes, S**, **Zawadowicz, MA**, **Pierce, JR**, **Shupe, MD**, **Schmale, J**, **Wang, J.** 2023. Arctic warming by abundant fine sea salt aerosols from blowing snow. *Nature Geoscience* **16**: 768–774. DOI: https://doi.org/10.1038/s41561-023-01254-8.

Halvorsen, MH, **Smedsrud, LH**, **Zhang, R**, **Kloster, K.** 2015. Fram Strait spring ice export and September Arctic sea ice. *The Cryosphere Discuss* **9**(4): 4205–4235. DOI: https://doi.org/10.5194/tcd-9-4205-2015.

Hanna, E, **Francis, J**, **Wang, M**, **Overland, JE**, **Cohen, J**, **Luo, D**, **Vihma, T**, **Fu, Q**, **Hall, RJ**, **Jaiser, R**, **Kim, S-J**, **Köhler, R**, **Luu, L**, **Shen, X**, **Erner, I**, **Ukita, J**, **Yao, Y**, **Ye, K**, **Choi, H**, **Skific, N.** 2024. Influence of high-latitude blocking and the northern stratospheric polar vortex on cold-air outbreaks under Arctic amplification of global warming. *Environmental Research: Climate* **3**(4): 042004. DOI: https://doi.org/10.1088/2752-5295/ad93f3.

Harris Stuart, R, **Faber, A-K**, **Wahl, S**, **Hörhold, M**, **Kipfstuhl, S**, **Vasskog, K**, **Behrens, M**, **Zuhr, AM**, **Steen-Larsen, HC.** 2023. Exploring the role of snow metamorphism on the isotopic composition of the surface snow at EastGRIP. *The Cryosphere* **17**(3): 1185–1204. DOI: https://doi.org/10.5194/tc-17-1185-2023.

Hersbach, H, **Bell, B**, **Berrisford, P**, **Hirahara, S**, **Horányi, A**, **Muñoz-Sabater, J**, **Nicolas, J**, **Peubey, C**, **Radu, R**, **Schepers, D**, **Simmons, A**, **Soci, C**, **Abdalla, S**, **Abellan, X**, **Balsamo, G**, **Bechtold, P**, **Biavati, G**, **Bidlot, J**, **Bonavita, M**, **De Chiara, G**, **Dahlgren, P**, **Dee, D**, **Diamantakis, M**, **Dragani, R**, **Flemming, J**, **Forbes, R**, **Fuentes, M**, **Geer, A**, **Haimberger, L**, **Healy, S**, **Hogan, RJ**, **Hólm, E**, **Janisková, M**, **Keeley, S**, **Laloyaux, P**, **Lopez, P**, **Lupu, C**, **Radnoti, G**, **De Rosnay, P**, **Rozum, I**, **Vamborg, F**, **Villaume, S**, **Thépaut, J-N.** 2020. The ERA5 global reanalysis. *Quarterly Journal of the Royal Meteorological Society* **146**(730): 1999–2049. DOI: https://doi.org/10.1002/qj.3803.

Jenkins, M, **Dai, A.** 2021. The impact of sea-ice loss on Arctic climate feedbacks and their role for Arctic amplification. *Geophysical Research Letters* **48**(15): e2021GL094599. DOI: https://doi.org/10.1029/2021GL094599.

Klein, ES, **Baltensperger, AP**, **Welker, JM.** 2024. Complexity of Arctic Ocean water isotope ($\delta^{18}O$, $\delta^{2}H$) spatial and temporal patterns revealed with machine learning. *Elementa: Science of the Anthropocene* **12**(1): 00127. DOI: https://doi.org/10.1525/elementa.2022.00127.

Klein, ES, **Cherry, JE**, **Young, J**, **Noone, D**, **Leffler, AJ**, **Welker, JM.** 2015. Arctic cyclone water vapor isotopes support past sea ice retreat recorded in Greenland ice. *Scientific Reports* **5**(1): 10295. DOI: https://doi.org/10.1038/srep10295.

Klein, ES, **Welker, JM.** 2016. Influence of sea ice on ocean water vapor isotopes and Greenland ice core records. *Geophysical Research Letters* **43**(24): 12475–12483. DOI: https://doi.org/10.1002/2016gl071748.

Knust, R. 2017. Polar research and supply vessel POLARSTERN operated by the Alfred-Wegener-Institute. *Journal of Large-Scale Research Facilities* **3**: A119. DOI: https://doi.org/10.17815/jlsrf-3-163.

Kopec, BG, **Feng, X**, **Michel, FA**, **Posmentier, ES.** 2016. Influence of sea ice on Arctic precipitation. *Proceedings of the National Academy of Sciences* **113**(1): 46–51. DOI: https://doi.org/10.1073/pnas.1504633113.

Kopec, BG, **Klein, ES**, **Feldman, GC**, **Pedron, SA**, **Bailey, H**, **Causey, D**, **Hubbard, A**, **Marttila, H**, **Welker, JM.** 2024. Arctic freshwater sources and ocean mixing relationships revealed with seawater isotopic tracing. *Journal of Geophysical Research: Oceans* **129**(7): e2023JC020583. DOI: https://doi.org/10.1029/2023JC020583.

Laepple, T, **Münch, T**, **Casado, M**, **Hoerhold, M**, **Landais, A**, **Kipfstuhl, S.** 2018. On the similarity and apparent cycles of isotopic variations in East Antarctic snow pits. *The Cryosphere* **12**(1): 169–187. DOI: https://doi.org/10.5194/tc-12-169-2018.

Legagneux, L, **Domine, F.** 2005. A mean field model of the decrease of the specific surface area of dry snow during isothermal metamorphism. *Journal of Geophysical Research: Earth Surface* **110**(F4). DOI: https://doi.org/10.1029/2004jf000181.

Leroy-Dos Santos, C, **Masson-Delmotte, V**, **Casado, M**, **Fourré, E**, **Steen-Larsen, HC**, **Maturilli, M**, **Orsi, A**, **Berchet, A**, **Cattani, O**, **Minster, B**, **Gherardi, J**, **Landais, A.** 2020. A 4.5 year-long record of Svalbard water vapor isotopic composition documents winter

air mass origin. *Journal of Geophysical Research: Atmospheres* **125**(23): e2020JD032681. DOI: https://doi.org/10.1029/2020jd032681.

Light, B, **Smith, MM**, **Perovich, DK**, **Webster, MA**, **Holland, MM**, **Linhardt, F**, **Raphael, IA**, **Clemens-Sewall, D**, **Macfarlane, AR**, **Anhaus, P**, **Bailey, DA.** 2022. Arctic sea ice albedo: Spectral composition, spatial heterogeneity, and temporal evolution observed during the MOSAiC drift. *Elementa: Science of the Anthropocene* **10**(1): 000103. DOI: https://doi.org/10.1525/elementa.2021.000103.

Liston, GE, **Polashenski, C**, **Rösel, A**, **Itkin, P**, **King, J**, **Merkouriadi, I**, **Haapala, J.** 2018. A distributed snow-evolution model for sea-ice applications (SnowModel). *Journal of Geophysical Research: Oceans* **123**(5): 3786–3810. DOI: https://doi.org/10.1002/2017jc013706.

Macfarlane, AR, **Dadic, R**, **Smith, MM**, **Light, B**, **Nicolaus, M**, **Henna-Reetta, H**, **Webster, M**, **Linhardt, F**, **Hämmerle, S**, **Schneebeli, M.** 2023a. Evolution of the microstructure and reflectance of the surface scattering layer on melting, level Arctic sea ice. *Elementa: Science of the Anthropocene* **11**(1): 00103. DOI: https://doi.org/10.1525/elementa.2022.00103.

Macfarlane, AR, **Mellat, M**, **Dadic, R**, **Meyer, H**, **Werner, M**, **Brunello, C**, **Arndt, S**, **Krampe, D**, **Schneebeli, M.** 2023b. Ocean-sourced snow: An unaccounted process on Arctic sea ice. Research Square Platform LLC. DOI: https://doi.org/10.21203/rs.3.rs-3572881/v1.

Macfarlane, AR, **Schneebeli, M**, **Dadic, R**, **Wagner, DN**, **Arndt, S**, **Clemens-Sewall, D**, **Hämmerle, S**, **Hannula, H-R**, **Jaggi, M**, **Kolabutin, N**, **Krampe, D**, **Lehning, M**, **Matero, I**, **Nicolaus, M**, **Oggier, M**, **Pirazzini, R**, **Polashenski, C**, **Raphael, I**, **Regnery, J**, **Shimanchuck, E**, **Smith, MM**, **Tavri, A**, **Mellat, M**, **Meyer, H**, **Werner, M**, **Brunello, CF.** 2022. Snowpit stable isotope profiles during the MOSAiC expedition [dataset]. PANGAEA. DOI: https://doi.org/10.1594/PANGAEA.952556.

Mellat, M, **Bailey, H**, **Mustonen, K-R**, **Marttila, H**, **Klein, ES**, **Gribanov, K**, **Bret-Harte, MS**, **Chupakov, AV**, **Divine, DV**, **Else, B**, **Filippov, I**, **Hyöky, V**, **Jones, S**, **Kirpotin, SN**, **Kroon, A**, **Markussen, HT**, **Nielsen, M**, **Olsen, M**, **Paavola, R**, **Pokrovsky, OS**, **Prokushkin, A**, **Rasch, M**, **Raundrup, K**, **Suominen, O**, **Syvänperä, I**, **Vignisson, SR**, **Zarov, E**, **Welker, JM.** 2021. Hydroclimatic controls on the isotopic ($\delta^{18}O$, $\delta^{2}H$, *d-excess*) traits of pan-Arctic summer rainfall events. *Frontiers in Earth Science* **9**(367): 651731. DOI: https://doi.org/10.3389/feart.2021.651731.

Mellat, M, **Brunello, CF**, **Werner, M**, **Bauch, D**, **Damm, E**, **Angelopoulos, M**, **Nomura, D**, **Welker, JM**, **Schneebeli, M**, **Granskog, MA**, **Hoerhold, M**, **Macfarlane, AR**, **Arndt, S**, **Meyer, H.** 2024. Isotopic signatures of snow, sea ice, and surface seawater in the central Arctic Ocean during the MOSAiC expedition. *Elementa: Science of the Anthropocene* **12**(1): 00078. DOI: https://doi.org/10.1525/elementa.2023.00078.

Mellat, M, **Meyer, H**, **Brunello, CF**, **Arndt, S**, **Macfarlane, AR**, **Schneebeli, M**, **Hörhold, M**, **Werner, M**, **Weiner, M**, **Marent, A.** 2022. Stable water isotopes of snow during MOSAiC expedition [dataset]. Bremerhaven, Germany: Alfred Wegener Institute for Polar and Marine Research. PANGAEA. DOI: https://doi.org/10.1594/PANGAEA.948511.

Merlivat, L, **Jouzel, J.** 1979. Global climatic interpretation of the deuterium-oxygen 18 relationship for precipitation. *Journal of Geophysical Research: Oceans* **84**(C8): 5029–5033. DOI: https://doi.org/10.1029/JC084iC08p05029.

Meyer, H, **Schönicke, L**, **Wand, U**, **Hubberten, HW**, **Friedrichsen, H.** 2000. Isotope studies of hydrogen and oxygen in ground ice—Experiences with the equilibration technique. *Isotopes in Environmental and Health Studies* **36**(2): 133–149. DOI: https://doi.org/10.1080/10256010008032939.

Moran, T, **Marshall, S.** 2009. The effects of meltwater percolation on the seasonal isotopic signals in an Arctic snowpack. *Journal of Glaciology* **55**(194): 1012–1024. DOI: https://doi.org/10.3189/002214309790794896.

Nandan, V, **Willatt, R**, **Mallett, R**, **Stroeve, J**, **Geldsetzer, T**, **Scharien, R**, **Tonboe, R**, **Yackel, J**, **Landy, J**, **Clemens-Sewall, D**, **Jutila, A**, **Wagner, DN**, **Krampe, D**, **Huntemann, M**, **Mahmud, M**, **Jensen, D**, **Newman, T**, **Hendricks, S**, **Spreen, G**, **Macfarlane, A**, **Schneebeli, M**, **Mead, J**, **Ricker, R**, **Gallagher, M**, **Duguay, C**, **Raphael, I**, **Polashenski, C**, **Tsamados, M**, **Matero, I**, **Hoppmann, M.** 2023. Wind redistribution of snow impacts the Ka- and Ku-band radar signatures of Arctic sea ice. *The Cryosphere* **17**(6): 2211–2229. DOI: https://doi.org/10.5194/tc-17-2211-2023.

Nicolaus, M, **Perovich, DK**, **Spreen, G**, **Granskog, MA**, **von Albedyll, L**, **Angelopoulos, M**, **Anhaus, P**, **Arndt, S**, **Belter, HJ**, **Bessonov, V**, **Birnbaum, G**, **Brauchle, J**, **Calmer, R**, **Cardellach, E**, **Cheng, B**, **Clemens-Sewall, D**, **Dadic, R**, **Damm, E**, **de Boer, G**, **Demir, O**, **Dethloff, K**, **Divine, DV**, **Fong, AA**, **Fons, S**, **Frey, MM**, **Fuchs, N**, **Gabarró, C**, **Gerland, S**, **Goessling, HF**, **Gradinger, R**, **Haapala, J**, **Haas, C**, **Hamilton, J**, **Hannula, H-R**, **Hendricks, S**, **Herber, A**, **Heuzé, C**, **Hoppmann, M**, **Høyland, KV**, **Huntemann, M**, **Hutchings, JK**, **Hwang, B**, **Itkin, P**, **Jacobi, H-W**, **Jaggi, M**, **Jutila, A**, **Kaleschke, L**, **Katlein, C**, **Kolabutin, N**, **Krampe, D**, **Kristensen, SS**, **Krumpen, T**, **Kurtz, N**, **Lampert, A**, **Lange, BA**, **Lei, R**, **Light, B**, **Linhardt, F**, **Liston, GE**, **Loose, B**, **Macfarlane, AR**, **Mahmud, M**, **Matero, IO**, **Maus, S**, **Morgenstern, A**, **Naderpour, R**, **Nandan, V**, **Niubom, A**, **Oggier, M**, **Oppelt, N**, **Pätzold, F**, **Perron, C**, **Petrovsky, T**, **Pirazzini, R**, **Polashenski, C**, **Rabe, B**, **Raphael, IA**, **Regnery, J**, **Rex, M**, **Ricker, R**, **Riemann-Campe, K**, **Rinke, A**, **Rohde, J**, **Salganik, E**, **Scharien, RK**, **Schiller, M**, **Schneebeli, M**, **Semmling, M**, **Shimanchuk, E**, **Shupe, MD**, **Smith,**

MM, **Smolyanitsky, V**, **Sokolov, V**, **Stanton, T**, **Stroeve, J**, **Thielke, L**, **Timofeeva, A**, **Tonboe, RT**, **Tavri, A**, **Tsamados, M**, **Wagner, DN**, **Watkins, D**, **Webster, M**, **Wendisch, M.** 2022. Overview of the MOSAiC expedition. *Elementa: Science of the Anthropocene* **10**(1): 000046. DOI: https://doi.org/10.1525/elementa.2021.000046.

Nixdorf, U, **Dethloff, K**, **Rex, M**, **Shupe, M**, **Sommerfeld, A**, **Perovich, DK**, **Nicolaus, M**, **Heuzé, C**, **Rabe, B**, **Loose, B**, **Damm, E**, **Gradinger, R**, **Fong, A**, **Maslowski, W**, **Rinke, A**, **Kwok, R**, **Spreen, G**, **Wendisch, M**, **Herber, A**, **Hirsekorn, M**, **Mohaupt, V**, **Frickenhaus, S**, **Immerz, A**, **Weiss-Tuider, K**, **König, B**, **Mengedoht, D**, **Regnery, J**, **Gerchow, P**, **Ransby, D**, **Krumpen, T**, **Morgenstern, A**, **Haas, C**, **Kanzow, T**, **Rack, FR**, **Saitzev, V**, **Sokolov, V**, **Makarov, A**, **Schwarze, S**, **Wunderlich, T**, **Wurr, K**, **Boetius, A.** 2021. MOSAiC extended acknowledgement. Zenodo. DOI: https://doi.org/10.5281/zenodo.5541624.

Nomura, D, **Kawaguchi, Y**, **Webb, AL**, **Li, Y**, **Dall'osto, M**, **Schmidt, K**, **Droste, ES**, **Chamberlain, EJ**, **Kolabutin, N**, **Shimanchuk, E**, **Hoppmann, M**, **Gallagher, MR**, **Meyer, H**, **Mellat, M**, **Bauch, D**, **Gabarró, C**, **Smith, MM**, **Inoue, J**, **Damm, E**, **Delille, B.** 2023. Meltwater layer dynamics in a central Arctic lead: Effects of lead width, re-freezing, and mixing during late summer. *Elementa: Science of the Anthropocene* **11**(1): 00102.

Nygård, T, **Papritz, L**, **Naakka, T**, **Vihma, T.** 2023. Cold wintertime air masses over Europe: Where do they come from and how do they form? *Weather and Climate Dynamics* **4**(4): 943–961. DOI: https://doi.org/10.5194/wcd-4-943-2023.

Pinzer, BR, **Schneebeli, M.** 2009. Snow metamorphism under alternating temperature gradients: Morphology and recrystallization in surface snow. *Geophysical Research Letters* **36**(23). DOI: https://doi.org/10.1029/2009gl039618.

Puntsag, T, **Mitchell, MJ**, **Campbell, JL**, **Klein, ES**, **Likens, GE**, **Welker, JM.** 2016. Arctic Vortex changes alter the sources and isotopic values of precipitation in northeastern US. *Scientific Reports* **6**(1): 22647. DOI: https://doi.org/10.1038/srep22647.

Rantanen, M, **Karpechko, AY**, **Lipponen, A**, **Nordling, K**, **Hyvärinen, O**, **Ruosteenoja, K**, **Vihma, T**, **Laaksonen, A.** 2022. The Arctic has warmed nearly four times faster than the globe since 1979. *Communications Earth & Environment* **3**(1): 168. DOI: https://doi.org/10.1038/s43247-022-00498-3.

Reinwarth, O, **Graf, W**, **Stichler, W**, **Moser, H**, **Oerter, H.** 1985. Investigations of the oxygen-18 content of samples from snow pits and ice cores from the Filchner-Ronne ice shelves and Ekström ice shelf. *Annals of Glaciology* **7**: 49–53. DOI: https://doi.org/10.3189/s0260305500005899.

Rinke, A, **Cassano, JJ**, **Cassano, EN**, **Jaiser, R**, **Handorf, D.** 2021. Meteorological conditions during the MOSAiC expedition: Normal or anomalous? *Elementa: Science of the Anthropocene* **9**(1): 00023. DOI: https://doi.org/10.1525/elementa.2021.00023.

Ritter, F, **Steen-Larsen, HC**, **Werner, M**, **Masson-Delmotte, V**, **Orsi, A**, **Behrens, M**, **Birnbaum, G**, **Freitag, J**, **Risi, C**, **Kipfstuhl, S.** 2016. Isotopic exchange on the diurnal scale between near-surface snow and lower atmospheric water vapor at Kohnen station, East Antarctica. *The Cryosphere* **10**(4): 1647–1663. DOI: https://doi.org/10.5194/tc-10-1647-2016.

Sinclair, KE, **Marshall, SJ.** 2008. Post-depositional modification of stable water isotopes in winter snowpacks in the Canadian Rocky Mountains. *Annals of Glaciology* **49**(1): 96–106. DOI: https://doi.org/10.3189/172756408787814979.

Smith, MM, **Angot, H**, **Chamberlain, EJ**, **Droste, ES**, **Karam, S**, **Muilwijk, M**, **Webb, AL**, **Archer, SD**, **Beck, I**, **Blomquist, BW**, **Bowman, J**, **Boyer, M**, **Bozzato, D**, **Chierici, M**, **Creamean, J**, **D'Angelo, A**, **Delille, B**, **Fer, I**, **Fong, AA**, **Fransson, A**, **Fuchs, N**, **Gardner, J**, **Granskog, MA**, **Hoppe, CJM**, **Hoppema, M**, **Hoppmann, M**, **Mock, T**, **Muller, S**, **Müller, O**, **Nicolaus, M**, **Nomura, D**, **Petäjä, T**, **Salganik, E**, **Schmale, J**, **Schmidt, K**, **Schulz, K**, **Shupe, MD**, **Stefels, J**, **Thielke, L**, **Tippenhauer, S**, **Ulfsbo, A**, **van Leeuwe, M**, **Webster, M**, **Yoshimura, M**, **Zhan, L.** 2023. Thin and transient meltwater layers and false bottoms in the Arctic sea ice pack—Recent insights on these historically overlooked features. *Elementa: Science of the Anthropocene* **11**(1): 00025. DOI: https://doi.org/10.1525/elementa.2023.00025.

Steen-Larsen, HC, **Masson-Delmotte, V**, **Hirabayashi, M**, **Winkler, R**, **Satow, K**, **Prié, F**, **Bayou, N**, **Brun, E**, **Cuffey, KM**, **Dahl-Jensen, D**, **Dumont, M**, **Guillevic, M**, **Kipfstuhl, S**, **Landais, A**, **Popp, T**, **Risi, C**, **Steffen, K**, **Stenni, B**, **Sveinbjörnsdottír, AE.** 2014. What controls the isotopic composition of Greenland surface snow? *Climate of the Past* **10**(1): 377–392. DOI: https://doi.org/10.5194/cp-10-377-2014.

Vérin, G, **Domine, F**, **Babin, M**, **Picard, G**, **Arnaud, L.** 2022. Metamorphism of snow on Arctic sea ice during the melt season: Impact on spectral albedo and radiative fluxes through snow. *The Cryosphere* **16**(9): 3431–3449. DOI: https://doi.org/10.5194/tc-16-3431-2022.

Vihma, T, **Screen, J**, **Tjernström, M**, **Newton, B**, **Zhang, X**, **Popova, V**, **Deser, C**, **Holland, M**, **Prowse, T.** 2016. The atmospheric role in the Arctic water cycle: A review on processes, past and future changes, and their impacts. *Journal of Geophysical Research: Biogeosciences* **121**(3): 586–620. DOI: https://doi.org/10.1002/2015jg003132.

Wagner, DN, **Shupe, MD**, **Cox, C**, **Persson, OG**, **Uttal, T**, **Frey, MM**, **Kirchgaessner, A**, **Schneebeli, M**, **Jaggi, M**, **Macfarlane, AR**, **Itkin, P**, **Arndt, S**, **Hendricks, S**, **Krampe, D**, **Nicolaus, M**, **Ricker, R**, **Regnery, J**, **Kolabutin, N**, **Shimanshuck, E**, **Oggier, M**, **Raphael, I**, **Stroeve, J**, **Lehning, M.** 2022. Snowfall and snow accumulation during the MOSAiC winter

and spring seasons. *The Cryosphere* **16**(6): 2373–2402. DOI: https://doi.org/10.5194/tc-16-2373-2022.

Wahl, S, **Steen-Larsen, HC**, **Hughes, AG**, **Dietrich, LJ**, **Zuhr, A**, **Behrens, M**, **Faber, AK**, **Hörhold, M.** 2022. Atmosphere-snow exchange explains surface snow isotope variability. *Geophysical Research Letters* **49**(20): e2022GL099529. DOI: https://doi.org/10.1029/2022gl099529.

Wahl, S, **Steen-Larsen, HC**, **Reuder, J**, **Hörhold, M.** 2021. Quantifying the stable water isotopologue exchange between the snow surface and lower atmosphere by direct flux measurements. *Journal of Geophysical Research: Atmospheres* **126**(13): e2020JD034400. DOI: https://doi.org/10.1029/2020jd034400.

Wahl, S, **Walter, B**, **Aemisegger, F**, **Bianchi, L**, **Lehning, M.** 2024. Identifying airborne snow metamorphism with stable water isotopes. *The Cryosphere* **18**(9): 4493–4515. DOI: https://doi.org/10.5194/tc-18-4493-2024.

Webster, M, **Gerland, S**, **Holland, M**, **Hunke, E**, **Kwok, R**, **Lecomte, O**, **Massom, R**, **Perovich, D**, **Sturm, M.** 2018. Snow in the changing sea-ice systems. *Nature Climate Change* **8**(11): 946–953. DOI: https://doi.org/10.1038/s41558-018-0286-7.

Yamanouchi, T, **Takata, K.** 2020. Rapid change of the Arctic climate system and its global influences: Overview of GRENE Arctic climate change research project (2011-2016). *Polar Science* **25**(9): 100548. DOI: https://doi.org/10.1016/j.polar.2020.100548.

Zhao, J, **Zhong, W**, **Diao, Y**, **Cao, Y.** 2019. The rapidly changing Arctic and its impact on global climate. *Journal of Ocean University of China* **18**(3): 537–541. DOI: https://doi.org/10.1007/s11802-019-3890-x.

Zuhr, AM, **Münch, T**, **Steen-Larsen, HC**, **Hörhold, M**, **Laepple, T.** 2021. Local-scale deposition of surface snow on the Greenland ice sheet. *The Cryosphere* **15**(10): 4873–4900. DOI: https://doi.org/10.5194/tc-15-4873-2021.

Zuhr, AM, **Wahl, S**, **Steen-Larsen, HC**, **Hörhold, M**, **Meyer, H**, **Laepple, T.** 2023. A snapshot on the buildup of the stable water isotopic signal in the upper snowpack at EastGRIP on the Greenland Ice Sheet. *Journal of Geophysical Research: Earth Surface* **128**(2): e2022JF006767. DOI: https://doi.org/10.1029/2022jf006767.

How to cite this article: Mellat, M, Macfarlane, AR, Brunello, CF, Werner, M, Schneebeli, M, Dadic, R, Arndt, S, Mustonen, K-R, Welker, JM, Divine, DV, Meyer, H. 2025. Arctic surface snow interactions with the atmosphere: Spatio-temporal isotopic variability during the MOSAiC expedition. *Elementa: Science of the Anthropocene* 13(1). DOI: https://doi.org/10.1525/elementa.2025.00028

Domain Editor-in-Chief: Detlev Helmig, Boulder AIR LLC, Boulder, CO, USA

Guest Editor: Zoe Courville, Thayer School of Engineering, Dartmouth, Hanover, NH, USA

Knowledge Domain: Atmospheric Science

Part of an Elementa Special Feature: The Multidisciplinary Drifting Observatory for the Study of Arctic Climate (MOSAiC)

Published: September 04, 2025 **Accepted:** July 7, 2025 **Submitted:** February 23, 2025

ELEMENTA Science of the Anthropocene

Elem Sci Anth is a peer-reviewed open access journal published by University of California Press.

OPEN ACCESS